Functional analyses of Pericentrin and Syne-2/Nesprin-2 interaction in ciliogenesis

Falk, Nathalie ; Kessler, Kristin ; Schramm, Sinja-Fee ; Boldt, Karsten ; Becirovic, Elvir ; Michalakis, Stylianos ; Regus-Leidig, Hanna ; Noegel, Angelika A ; Ueffing, Marius ; Thiel, Christian T ; Roepman, Ronald ; Brandstätter, Johann Helmut ; Gießl, Andreas

DOI: https://doi.org/10.1242/jcs.218487

© 2018. Published by The Company of Biologists Ltd | Journal of Cell Science (2018) 131, jcs218487. doi:10.1242/jcs.218487

RESEARCH ARTICLE

Functional analyses of Pericentrin and Syne-2 interaction in ciliogenesis

Nathalie Falk[1], Kristin Kessler[1], Sinja-Fee Schramm[1], Karsten Boldt[2], Elvir Becirovic[3], Stylianos Michalakis[3], Hanna Regus-Leidig[1], Angelika A. Noegel[4], Marius Ueffing[2], Christian T. Thiel[5], Ronald Roepman[6], Johann Helmut Brandstätter[1] and Andreas Gießl[1,*]

ABSTRACT

Pericentrin (Pcnt) is a multifunctional scaffold protein and mutations in the human *PCNT* gene are associated with several diseases, including ciliopathies. Pcnt plays a crucial role in ciliary development in olfactory receptor neurons, but its function in the photoreceptor-connecting cilium is unknown. We downregulated Pcnt in the retina *ex vivo* and *in vivo* via a virus-based RNA interference approach to study Pcnt function in photoreceptors. ShRNA-mediated knockdown of Pcnt impaired the development of the connecting cilium and the outer segment of photoreceptors, and caused a nuclear migration defect. In protein interaction screens, we found that the outer nuclear membrane protein Syne-2 (also known as Nesprin-2) is an interaction partner of Pcnt in photoreceptors. Syne-2 is important for positioning murine photoreceptor cell nuclei and for centrosomal migration during early ciliogenesis. CRISPR/Cas9-mediated knockout of Syne-2 in cell culture led to an overexpression and mislocalization of Pcnt and to ciliogenesis defects. Our findings suggest that the Pcnt–Syne-2 complex is important for ciliogenesis and outer segment formation during retinal development and plays a role in nuclear migration.

KEY WORDS: Pericentrin, Syne-2, Nuclear migration, Primary cilium, Ciliogenesis, Retina, CRISPR/Cas9

INTRODUCTION

Pericentrin (Pcnt), also known as kendrin, is a major component of the pericentriolar material (PCM) functioning in a diverse repertoire of biological processes (Doxsey et al., 1994; for a review, see Delaval and Doxsey, 2010). The large coiled-coil protein is encoded by orthologous genes in mice and humans with three known splice variants described so far: Pcnt B (360), Pcnt A and Pcnt S (250) (Flory and Davis, 2003; Miyoshi et al., 2006a; see Materials and Methods for further details). Pcnt has previously been localized to the centrosome, the microtubule organizing center of cycling cells (Miyoshi et al., 2006b). The centrosomal localization of Pcnt is mediated by a pericentrosomal matrix targeting motif, called the PACT [pericentrin-AKAP450 (AKAP9) centrosomal targeting] domain in its C-terminus (Doxsey et al., 1994; Gillingham and Munro, 2000). Coinciding with the PCM, Pcnt is also present at the base of primary and motile cilia (Jurczyk et al., 2004; Miyoshi et al., 2006b). Pcnt serves as a multifunctional scaffold for numerous proteins and contributes to a diversity of fundamental cellular processes, such as mitotic spindle organization, the DNA damage response and primary cilia formation (Zimmerman et al., 2004; Jurczyk et al., 2004; Tibelius et al., 2009). Mutations in the human *PCNT* gene are associated with pleiotropic defects, including primordial dwarfism, cancer, schizophrenia and ciliopathies (Rauch et al., 2008; Griffith et al., 2008; Piane et al., 2009; Delaval and Doxsey, 2010; Chen et al., 2014). Pcnt exerts important functions during ciliogenesis in cultured human epithelial cells and in the mouse olfactory epithelium. However, its function in other sensory neurons, e.g. the photoreceptors in the retina remains unclear (Jurczyk et al., 2004; Miyoshi et al., 2009).

A vertebrate photoreceptor comprises a biosynthetic and metabolic active inner segment (IS), which is linked via a narrow microtubule-based intracellular bridge, the connecting cilium, to the photoreceptive outer segment (OS) containing the opsin-loaded outer segment membrane discs. These latter two regions represent the photoreceptor sensory cilium, which is separated from the cytosol by its centriole-derived basal body (Roepman and Wolfrum, 2007; Gilliam et al., 2012). Previously, we have shown that in the mouse retina Pcnt splice variants are specifically localized to the basal body complex (BBC) of the photoreceptor connecting cilium (CC) and at the centrosomes of other retinal cell types (Mühlhans et al., 2011; Falk et al., 2015). In the present study, we performed interaction trap screens in yeast (two-hybrid system) to identify binary interaction partners of Pcnt to gain deeper insight into the function of Pcnt in mouse retina. One interaction partner of Pcnt was the nuclear envelope protein Syne-2, which plays a role in nuclear migration and positioning during retinal development in several species (Patterson et al., 2004; Tsujikawa et al., 2007; Yu et al., 2011), as well as in ciliogenesis (Dawe et al., 2009). Downregulation of *Pcnt* caused defects in nuclear migration and disrupted the development of the CC and the adjacent photoreceptor OS. Experiments addressing the colocalization of Pcnt and Syne-2 and CRISPR/Cas9 knockout experiments in cell lines suggest that the interaction of Pcnt with Syne-2 is required for ciliogenesis in differentiated cells, as well as for the attachment of the centrosome to the nucleus in cycling cells, which is critical for correct nuclear migration and cell polarization in the retina.

[1]Animal Physiology, Friedrich-Alexander-Universität Erlangen-Nürnberg, 91058 Erlangen, Germany. [2]Division of Experimental Ophthalmology and Medical Proteome Center, Center of Ophthalmology, University of Tübingen, 72074 Tübingen, Germany. [3]Center for Integrated Protein Science Munich (CIPSM) at the Department of Pharmacy, Center for Drug Research, Ludwig-Maximilians-Universität München, 81377 Munich, Germany. [4]Institute of Biochemistry I, Medical Faculty, University Hospital, University of Cologne, 50931 Cologne, Germany. [5]Institute of Human Genetics, Friedrich-Alexander-Universität Erlangen-Nürnberg, 91054 Erlangen, Germany. [6]Department of Human Genetics, Radboud University Medical Center, Nijmegen 6525 GA, The Netherlands.

*Author for correspondence (andreas.giessl@fau.de)

N.F., 0000-0001-6722-0292; S.-F.S., 0000-0002-8453-2033; K.B., 0000-0002-2693-689X; E.B., 0000-0001-8801-0649; S.M., 0000-0001-5092-9238; H.R.-L., 0000-0002-5004-8534; A.A.N., 0000-0001-8260-6732; M.U., 0000-0003-2209-2113; C.T.T., 0000-0003-3817-7277; R.R., 0000-0002-5178-8163; J.H.B., 0000-0002-6468-5585; A.G., 0000-0002-9768-2049

Received 29 March 2018; Accepted 12 July 2018

Journal of Cell Science (2018) 131, jcs218487. doi:10.1242/jcs.218487

RESULTS

Knockdown of Pcnt affects cell division and ciliogenesis in mouse cell lines

For Pcnt knockdown in rod photoreceptors, we used lenti- and adeno-associated virus-based RNA interference approaches. To ensure knockdown of the currently known Pcnt splice variants, the target sequences for lentiviral shRNAs 3947, 4777 and 5248, and for AAV shRNAs 3491 and 4285 were selected from the middle portion of Pcnt (Fig. 1A). The knockdown efficiencies of the different shRNAs were first tested in cultured NIH 3T3 mouse embryonic fibroblasts by quantitative PCR. Normalized Pcnt mRNA levels in cells transfected with the single shRNAs were reduced by 15-30% (Fig. 1B). The relatively low knockdown efficiency correlates with the transfection efficiency (<30%) of these cells.

Compared with immunofluorescence staining in control cells, staining of shRNA-transfected NIH 3T3 mouse fibroblasts for Pcnt and α-tubulin in combination with nuclear staining (DAPI) revealed a reduction of Pcnt at the centrosome (identified by GFP fluorescence, Fig. 1C-F). Furthermore, we observed a cell cycle arrest in the G1 phase (Mikule et al., 2007), and occasionally, multiple cell nuclei and supernumerary centrosomes (Chen et al., 2004). To assess the potential effects of Pcnt knockdown on cilia formation, we used murine inner medullary collecting duct 3 (mIMCD3) cells, in which the formation of primary cilia can be induced by starvation (Wheway et al., 2015). The lenti- and adeno-associated virus-based shRNA constructs expressed an eGFP reporter that enabled the identification of transduced cells. The shRNA-dependent effects on ciliogenesis were quantified from the transduced cells. Knockdown of Pcnt in starved mIMCD3 cells led to primary cilia assembly in 33-45% of the shRNA cells ($n \geq 180$), depending on the shRNA used, compared with 63% in the scramble shRNA control cells ($n \geq 180$) (Fig. 1G). The observed reduction in cilia numbers is comparable to the results from Pcnt knockdown experiments in human epithelial cells (Jurczyk et al., 2004).

Knockdown of Pcnt affects rod photoreceptor morphology

To study the effect of Pcnt knockdown on mouse retina, we transduced *in vitro* organotypic mouse retina cultures with lentiviral shRNA viruses between postnatal day (P)0 and P1. In addition, we performed an *in vivo* knockdown of Pcnt via subretinal injection of adeno-associated shRNA viruses between P5 and P7. The impact of Pcnt knockdown on retina morphology was analyzed with

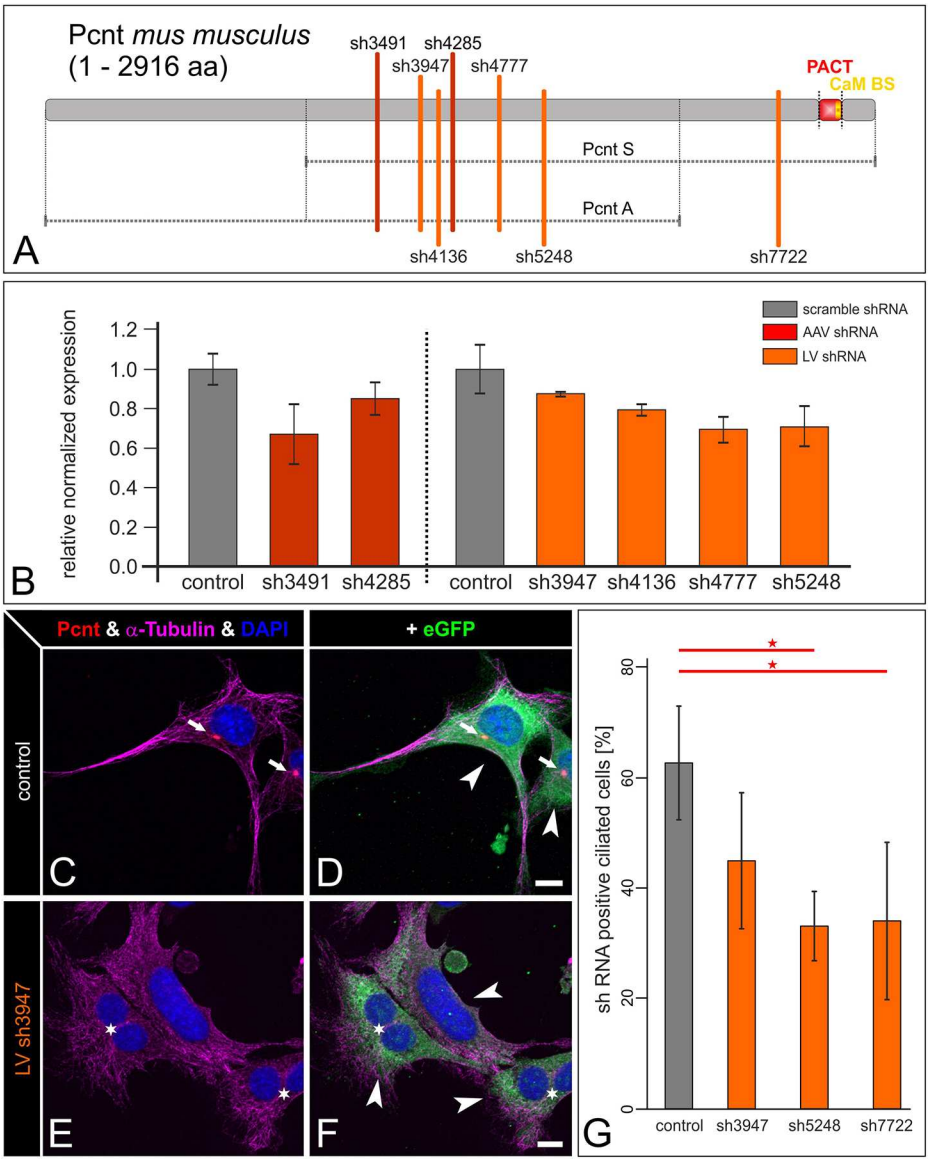

Fig. 1. ShRNA knockdown of Pcnt in mouse NIH 3T3 and IMCD3 cells. (A) Scheme of Pcnt splice variants Pcnt B [360, accession number (AN): NP_032813.3], Pcnt A (AN: partial, AAO24322.1) and Pcnt S (250, BAF36560.1) and the positions of the shRNAs used for Pcnt knockdown. (B) Quantitative PCR of Pcnt (amplified fragment present in these splice variants) in the transfected 3T3 cell line normalized to the scrambled shRNA control. (C-F) Quadruple labeling of eGFP (green; arrowheads indicate transduced cells), Pcnt (red, arrows), α-tubulin (magenta) and DAPI in scrambled (control, C,D) and Pcnt (E,F) shRNA-transfected 3T3 mouse embryonic fibroblasts. Downregulation of Pcnt showed different phenotypes in cell culture (E,F), with reduced Pcnt staining, often multiple cell nuclei (asterisks in E,F) and sometimes supernumerary centrosomes. (G) Quantification of cells with cilia in shRNA-transfected IMCD3 cells and control cells kept in starved medium (72 h) to induce ciliation (n>120 cells; eGFP used as a reporter). Knockdown of Pcnt significantly reduced the number of ciliated cells (Shapiro–Wilk test and t-test: *P<0.05); values are mean±s.d. of n=5. Scale bars: 10 µm.

Journal of Cell Science (2018) 131, jcs218487. doi:10.1242/jcs.218487

light and electron microscopy. For light microscopy analysis, we immunostained vertical cryostat sections of transduced and control retinas with antibodies against GFP and rhodopsin. Knockdown of Pcnt led to a disorganized outer retinal structure in combination with cell nuclei mislocalized from the outer nuclear layer to the region of the inner (IS) and outer (OS) photoreceptor segments both *in vitro* and *in vivo* (Fig. 2A-E). The photoreceptor-connecting cilia were either truncated or completely absent (Fig. 2F-J). Moreover, we observed photoreceptor degeneration and absence of photoreceptor OSs in Pcnt shRNA-treated retinas. To exclude off-target effects of the viral transduction or GFP expression, GFP and scramble shRNA-transduced retinas were analyzed as a control. Importantly, no differences in outer retinal structure could be detected comparing transduced and non-transduced retinal areas (Fig. S1).

Interaction screens identify interaction of Pcnt with Syne-2

Several interaction partners of Pcnt have previously been identified at centrosomal and ciliary structures, including the centrosomal and Golgi N-kinase anchoring protein (CG-NAP), pericentriolar material 1 (PCM1), disrupted-in-schizophrenia 1 (DISC1), intraflagellar transport 20 (IFT20) and polycystin-2 (PC2), suggesting the involvement of Pcnt in a multitude of fundamental cellular processes (Delaval and Doxsey, 2010).

To further investigate the Pcnt interactome, we performed tandem affinity purification (TAP) combined with mass spectrometry (MS) (Gloeckner et al., 2007). Five Pcnt protein fragments covering the known splice variants and domains were fused to an N- and C-terminal Strep-FLAG tag (NTAP) and expressed in HEK293T cells (Fig. 3A). MS analysis of the purified protein complexes identified a total of 746 unique, co-purified proteins (without false-positive proteins and proteins identified in the control, but no filter methods). The already reported interactors PCM1, calmodulin and CDK5 regulatory subunit-associated protein 2 (Cdk5rap2) were also present in the purified protein network, validating the specificity of our approach (Li et al., 2001; Gillingham and Munro, 2000; Buchman et al., 2010).

To further validate the Pcnt interactions, we conducted an additional yeast two-hybrid screen (Y2H) utilizing our mouse retinal cDNA library (first described in Gotthardt et al., 2015). To this end, we generated five Pcnt fragments corresponding to those described in Fig. 3A. Only Pcnt part 4 showed noticeable levels of auto-activation, and consequently, this fragment was excluded from the screen. The library screening produced several clones growing on selective medium. Sequencing of the single clones revealed several potential Pcnt-interacting proteins. Among the Pcnt interactors identified in the TAP and Y2H screen, we specifically focussed on proteins whose functional and localization profile was similar to that of Pcnt. Syne-2 (NM_001005510.2; ENSMUST00000044217) was found to be the most promising interaction partner of Pcnt (Fig. 3C). It was identified 17 times (peptide) in three independent TAP screens and 19 times in Y2H screens (Fig. 3B). Syne-2 was shown previously to be involved in nuclear migration and ciliogenesis; and knockout (KO) of Syne-2 leads to retinal degeneration (Dawe et al., 2009; Yu et al., 2011). The TAP screen, which cannot distinguish between direct and indirect interactions, revealed an interaction between Pcnt part 1, 2 or 3 and Syne-2. The subsequent Y2H screen confirmed a direct interaction with Pcnt part 2 and 5 (2/5). The Syne-2 fragment identified in the Y2H screen corresponds to the residues 1921-2066 encoded by exons 39-41 (Fig. 3B). Since Pcnt part 1 and part 3 have not been identified in the Y2H screen, it seems reasonable to assume that these fragments do not directly bind to Syne-2. To confirm and to quantify the Pcnt–Syne-2 interaction in another independent approach, we performed a binary Y2H analysis (1-on-1 assay) using Pcnt part 2/5 and the Syne-2 construct comprising residues 1852-2143 encoded by exons 38-43 (Fig. 3B). To verify the positive Y2H interactions, we switched prey and bait constructs (Pcnt part 2/5 bait to prey and Syne-2 prey to bait). Auto-activation of the Pcnt constructs was excluded (Fig. 3F). In addition, 1-on-1 Y2H analyses in two single X-α-galactosidase and liquid β-galactosidase assays were performed (Fig. 3D,E). Pcnt part 2/5 and Syne-2 developed a dark blue color on high-stringency plates with X-α-Gal, indicating strong interactions (Fig. 3D). As a reference for a high binding

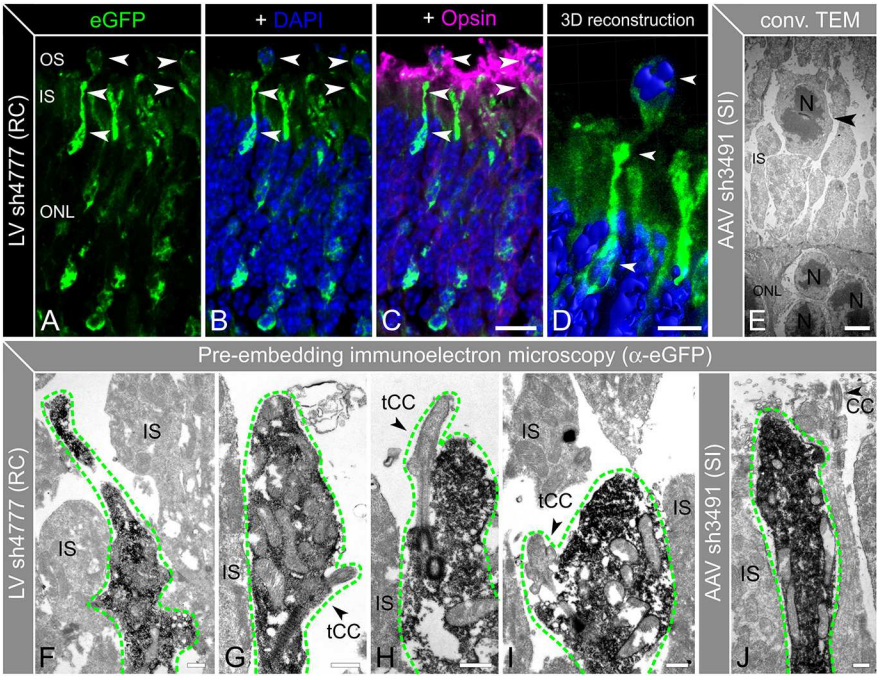

Fig. 2. Phenotype of *ex vivo*/*in vivo* shRNA knockdown of Pcnt in the developing retina. (A-C) Triple labeling of eGFP (green; arrowheads indicate transduced cells), DAPI (blue) and Opsin (magenta) of a lentivirus shRNA (LV) transduced organotypic mouse retina culture. Outer retina structure was often disorganized and cell nuclei in the part of the photoreceptors inner segments (IS) and outer segments (OS, arrowheads, see 3D reconstruction in D) were mislocalized. (E) Unstained conventional transmission electron microscopy image of an eye injected with shRNA expressing AAV (SI) showing a mislocalized cell nucleus (arrowhead). (F-I) Electron micrographs (pre-embedding labeling with antibody against eGFP) showing the ultrastructural localization of eGFP in shRNA transduced photoreceptor inner segments (IS; green dotted line) from organotypic mouse retina culture. (J) Electron micrograph showing the ultrastructural localization of eGFP in a shRNA-transduced photoreceptor inner segment (IS; green dotted line) from an AAV-transduced mouse retina. CC, connecting cilium; tCC, truncated connecting cilium; ONL, outer nuclear layer. Scale bars: 10 µm (C), 5 µm (D), 2 µm (E) and 0.5 µm (F-J).

Journal of Cell Science (2018) 131, jcs218487. doi:10.1242/jcs.218487

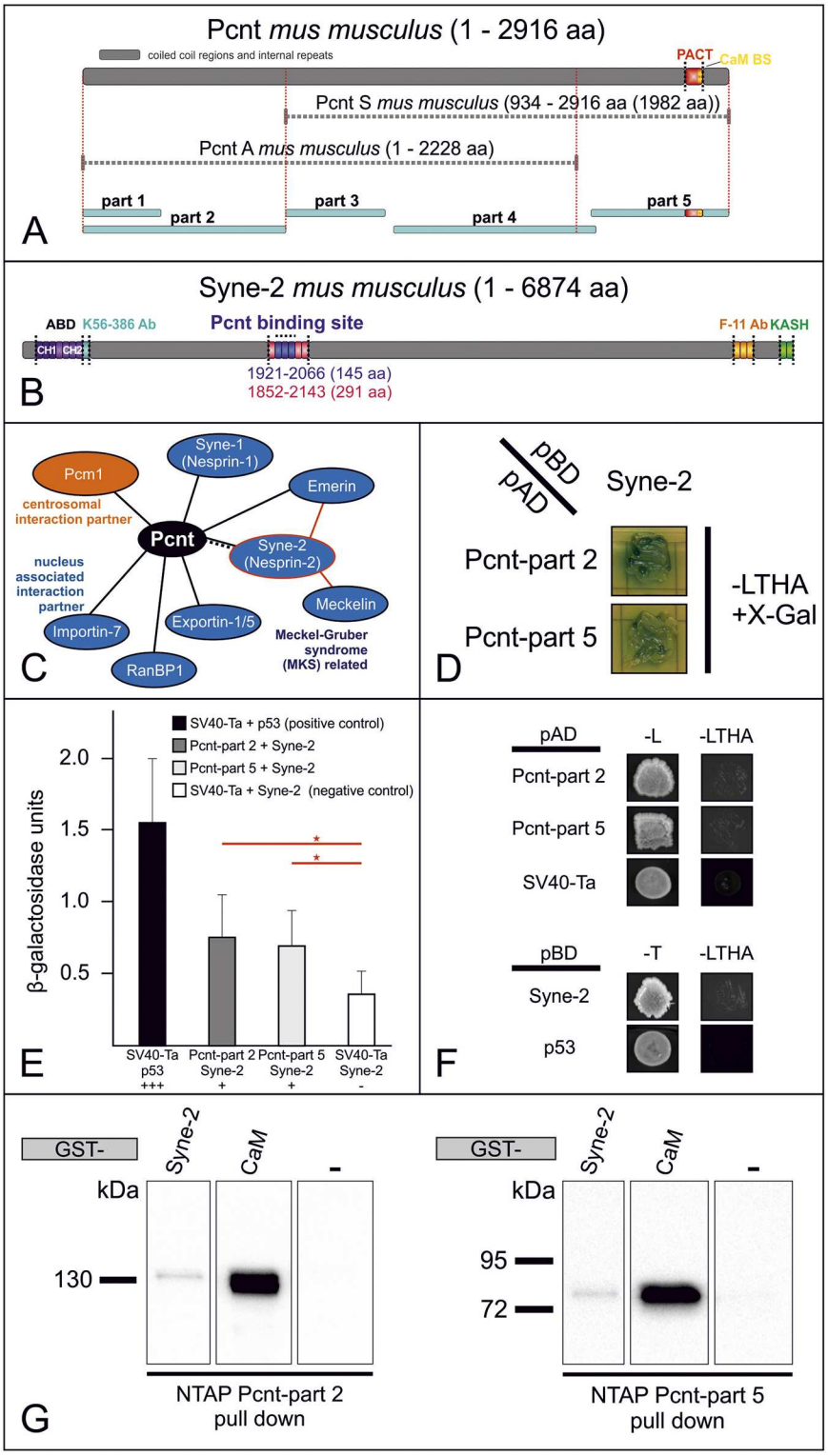

Fig. 3. Confirmation of Syne-2 as interaction partner of Pcnt. (A) Scheme of the Pcnt splice variants: Pcnt B, Pcnt A and Pcnt S (see Fig. 1A) containing the pericentrin-AKAP450 (AKAP9) centrosomal targeting domain (PACT domain) and a calmodulin binding site (CaM BS). In light blue, Pcnt parts 1-5 are illustrated, which were used in the tandem affinity purification and yeast two-hybrid screen. (B) Schematic structure of the Syne-2 protein (NM_001005510.2; ENSMUST00000044217) containing an N-terminal actin-binding domain (ABD) and a C-terminal Klarsicht, ANC-1 and Syne homology (KASH) domain. The localization of the Pcnt binding site (exon 39-41, aa residues 1921-2066) and epitopes of anti-Syne-2 antibodies are indicated. (C) Detailed interaction network of Pcnt with the focus on nucleus-associated binding partners and Pcm-1. Included are the data of the TAP (black lines) and the yeast two-hybrid screen (black dashed line), and interactions known from the literature (red lines) (Zhang et al., 2005; Dawe et al., 2009). (D) α-galactosidase assay between Pcnt part 2/5-pAD and Syne-2-pBD. Transformed and mated cells were grown on high-stringency plates (–LTHA+X-Gal). (E) The strength of the interaction was quantified by performing a β-galactosidase assay. The β-galactosidase activity of Pcnt part 2/5 and Syne-2 (0.76±0.29/0.69±0.25, respectively) were significantly stronger than that of the SV40-TA/Syne-2 negative control (0.37±0.16). Positive control, SV40-Ta-pAD and p53-pBD (1.55±0.45); values are mean±s.d.; **P*<0.005, *n*=5, Shapiro-Wilk test and *t*-test. (F) Constructs did not show any growth on minimal medium except -L (pAD) and -T (pBD). (G) GST-Syne-2 efficiently pulled down NTAP Pcnt part 2 (~130 kDa) and NTAP Pcnt part 5 (~80 kDa). Unfused GST failed to pull down NTAP Pcnt part 2/5 (Input: 18.75% of the PD). Positive control, calmodulin (CaM).

affinity in this assay, the well-described interaction between the SV40 large T antigen (SV40-TA in pGADT7) and the tumor suppressor protein p53 (p53 in pGBKT7) was used (Croci et al., 2003). As a negative control, SV40-TA in pGADT7 with the screened Pcnt interaction partner Syne-2 in pGBKT7 was used. Based on the β-galactosidase units (colorimetric assay), the relative interaction strength between the proteins could be determined. The β-galactosidase activity of Pcnt part 2/5 and Syne-2 was significantly higher than that of the SV40-TA and Syne-2 negative control (Fig. 3E; Shapiro–Wilk test and *t*-test: $P<0.05$). The binary Y2H results confirmed the interaction between Pcnt part 2/5 and the Syne-2 fragment obtained in the global Y2H screen.

To further assess the interaction between Pcnt part 2/5 and Syne-2 *in vitro*, we performed a GST pull-down assay. Bacterially expressed GST-fused Syne-2 efficiently pulled down ectopically expressed NTAP-Pcnt part 2/5 from lysates of HEK293T cells, validating the Pcnt–Syne-2 interaction (Fig. 3G). As a positive control, the interaction between NTAP-Pcnt part 2/5 and GST-calmodulin was

Journal of Cell Science (2018) 131, jcs218487. doi:10.1242/jcs.218487

used. GST-Syne-2 did not interact with NTAP-calmodulin (data not shown) nor did NTAP-Pcnt part 2/5 bind to unfused GST, validating the specificity of the detected interaction (Fig. 3G).

Syne-2 localizes to the basal body complex of the photoreceptor connecting cilium

In mouse photoreceptor cells, Syne-2 was shown to be crucial for proper retinal structure and function (Tsujikawa et al., 2007; Yu et al., 2011); however, little is known about the distribution pattern of Syne-2 in the vertebrate retina. First, we assessed whether Pcnt and Syne-2 colocalize in the adult mouse retina. We stained retinal cryostat sections using the specific monoclonal Syne-2 antibody K56-386 (Fig. 4). The antibody specifically stained the nuclear envelope of the cells in the outer nuclear layer (ONL), the inner nuclear layer (INL) and the ganglion cell layer (GCL), which is due to the anchorage of Syne-2 in the outer nuclear membrane via the C-terminal KASH domain (Dawe et al., 2009). Importantly, robust Syne-2 signal was found throughout the metabolically active IS of the photoreceptors (Fig. 4A,C,C′). Double labeling with the Pcnt specific antibody MmPeriC1 and high-resolution image of the ciliary region (Fig. 4C′) further revealed that Syne-2 and Pcnt partially colocalizes at the basal body complex of the CC in the IS of photoreceptors. To examine a possible interaction of the two proteins at the connecting cilium, we performed *in situ* proximity ligation assays (PLA; (Gustafsdottir et al., 2005; Söderberg et al., 2006) on vertical retinal cryostat sections in mice (Fig. 4D,E). We obtained a strong PLA signal at the basal body complex of the CC (Fig. 4D,E), suggesting a potential interaction of Pcnt and Syne-2 at the basal body complex in the IS of mouse photoreceptor cells (Fig. 4F).

CRISPR/Cas9 knockout of Syne-2 in mIMCD3 cells affects ciliogenesis and cilia length

We chose an *in vitro* cell culture system to study the interaction between Pcnt and Syne-2 (binding site Syne-2, exon 39-41, N-terminal), because: (1) the complete knockout of Pcnt in mice ($Pcnt^{m239Asp}$, MGI) results in perinatal lethality (Endoh-Yamagami et al., 2010) and (2) C-terminal (KASH domain)-deleted Syne-2 mice ($Syne\text{-}2^{tm1Rexu}$, MGI) reported to have a retinal phenotype (Yu et al., 2011) are no longer available (originally available from Prof. Min Han, University of Colorado, USA). To determine the function of Syne-2 on a cellular level, we generated clonal *Syne2* KO cell lines using CRISPR/Cas9-based genome editing. For this purpose, we used CRISPR RNA-guided Cas9 nucleases with target sites in exons 39 and 41 of *Syne2* (Table S1). Three homozygous clones showed homozygous indel mutations in exon 39 (S30 and S52) or in exon 41 (S112) (Fig. 5A,B and Fig. S2A,B). The affected positions are highly conserved at the nucleotide and amino acid level. No mutations were identified in the non-target control (C2 NT). Immunoblotting with the C-terminal anti-Syne-2 antibody ($Syne\text{-}2^{C\text{-}term}$, F11) confirmed the complete absence of the full-length Syne-2 protein in the KO clones compared with Syne-2 expression in the non-target control (C2 NT) (Fig. 5C,D). Immunolabeling of the KO cells using the C-terminal antibody showed that Syne-2 was completely absent in the outer nuclear envelope (Fig. 5E-G′). Syne-2 localization appeared normal in control WT C2 NT cells (Fig. 5H,H′).

As Syne-2 is suggested to be involved in cilia formation (Dawe et al., 2009), we performed immunofluorescence staining and analyzed ciliogenesis in *Syne2*-depleted cells. In WT control cells, 72 h of starvation triggered cilia formation in 52% of the cells, whereas in Syne-2 KO cell lines with deletions in exon

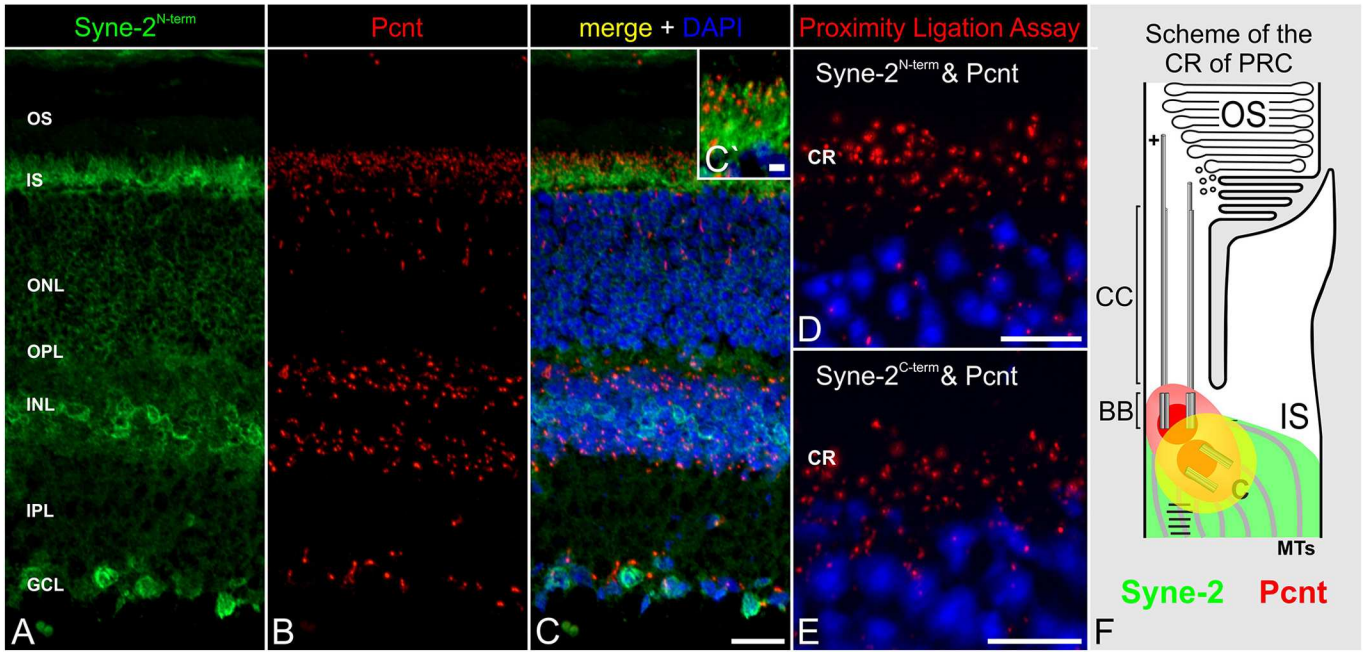

Fig. 4. Localization of Syne-2 and putative interaction with Pcnt in the inner segment of mouse photoreceptors. (A-C) Images of vertical sections through an adult C57BL/6JRj mouse retina, stained with antibodies against $Syne\text{-}2^{N\text{-}term}$ (K56-386, green) and Pcnt (MmPeriC1, red), and DAPI (blue) as a nuclear marker. (A) Syne-2 is localized in the inner segment (IS) of photoreceptors and in the outer nuclear membrane of retinal cells in the outer nuclear layer (ONL), inner nuclear layer (INL) and ganglion cell layer (GCL). (B) Pcnt is present at the basal body complex (BBC) of the photoreceptor-connecting cilia and at the centrosomes of non-photoreceptor cells in the ONL, INL and GCL. (C′) High-magnification image showing overlap of Syne-2 and Pcnt staining at the BBC of the connecting cilium in the IS of photoreceptors. (D,E) $Syne2^{N\text{-}term}$-Pcnt (D) and $Syne2^{C\text{-}term}$-Pcnt (E) interactions (red dots) are detected by proximity ligation assay (PLA) in the ciliary region (CR), signifying a putative protein-protein interaction. (F) Scheme summarizing the subcellular localization and the interaction area (yellow) of Pcnt and Syne-2 in the photoreceptor CR. OS, outer segment; OPL, outer plexiform layer; IPL, inner plexiform layer; BB, basal body; C, centriole; MTs, microtubules; PRC, photoreceptor cell. Scale bars: 20 µm (C), 2 µm (C′), 10 µm (D,E).

Journal of Cell Science (2018) 131, jcs218487. doi:10.1242/jcs.218487

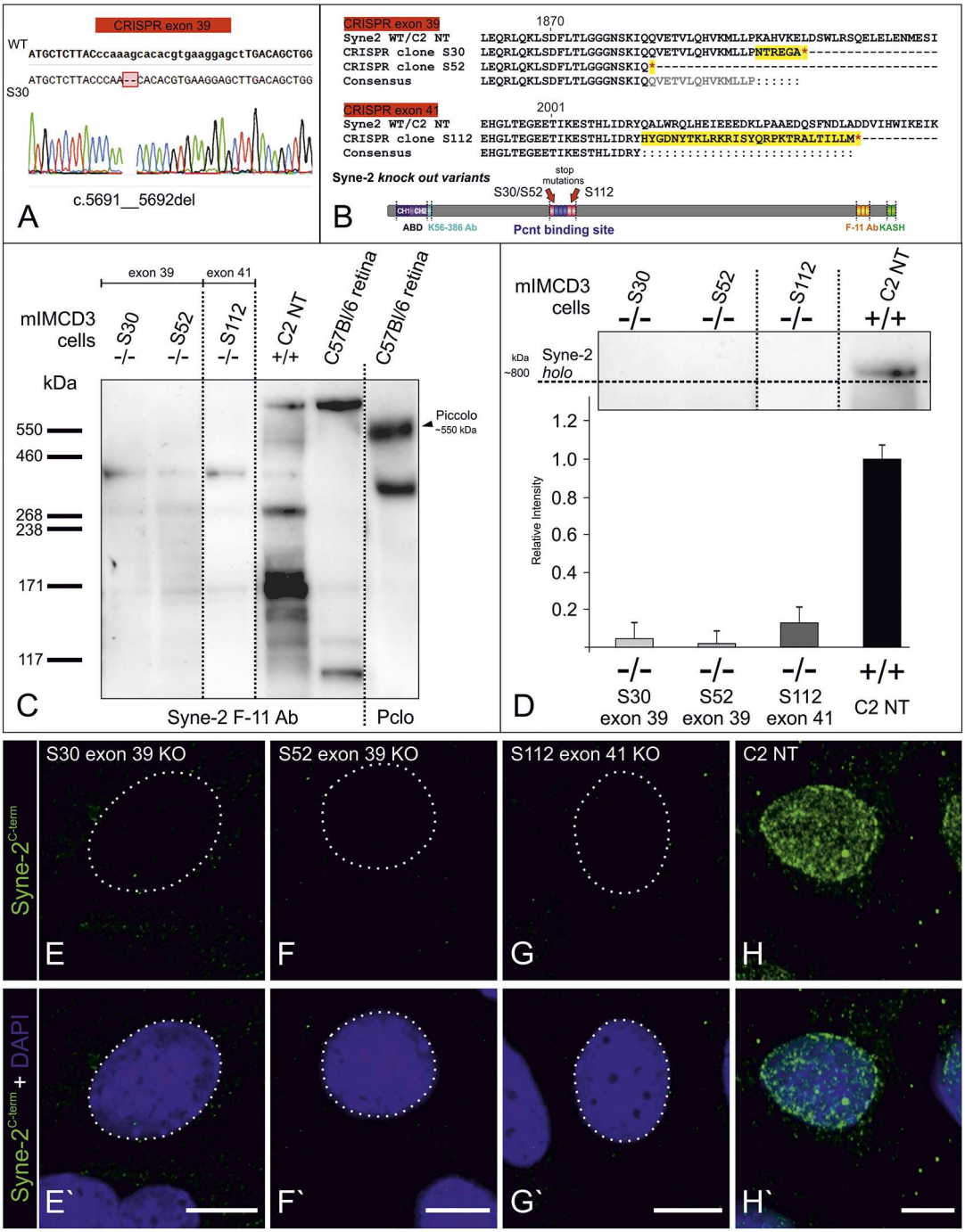

Fig. 5. Generation of Syne-2-knockout cell lines by CRISPR/Cas9. (A) Sequence alignment of bases 5678-5719 of the RefSeqGene mouse *Syne2* (NM_001005510.2) and a mutant allele of Syne-2 KO clone S30 showing a homozygous 2 bp deletion bounded by a red box (B) Sequence alignment of non-target control (C2 NT/WT) and homozygous Syne-2 KO clones targeting exon 39 (S30, S52) and exon 41 (S112). Syne-2 KO cell lines were confirmed by direct sequencing of PCR products. Schematic protein structure of the Syne-2 protein (NM_001005510.2; ENSMUST00000044217) illustrating the stop mutations (red arrow) of the CRISPR Syne-2 KO cell lines S30/S52 (without Pcnt binding site) and S112 (including Pcnt binding site). (C) Depletion of the Syne-2 protein in KO cell lines was confirmed by immunoblotting with an anti-Syne-2 antibody. An anti-Piccolo antibody detecting Piccolo was used for validating protein sizes (550 kDa). (D) Micrograph of the mean band intensity measurement of the Syne-2-stained western blot holo band normalized to total protein with stain-free technique (Bio-Rad) and compared with control (C2 NT, n=5). The generated Syne-2 KO cells lines show a complete loss of full-length Syne-2 (796 kDa). (E-H) Immunofluorescence staining of Syne-2 KO cell lines [S30 (E,E′), S52 (F,F′) and S112 (G,G′)] and non-target control [C2 NT (H,H′)] with an antibody against Syne-2 (green, C-term mAb F-11) and DAPI (blue, nuclear marker). In KO cell lines, Syne-2 staining was not detectable in the outer nuclear membrane (E-G′), but is clearly seen in WT nuclei (H,H′). Scale bars: 10 µm (E′-H′).

39 (S30, S52), only 17-19% of the cells were ciliated (Fig. 6A-C′,E). Surprisingly, the Syne-2 KO S112 cell line with the deletion in exon 41 remained unaffected (53% ciliated cells, Fig. 6D,D′,E). However, the KO cell lines showed a significant reduction of cilia length compared with the WT control line (S30=0.97 µm, S52=1.02 µm, S112=1.72 µm, WT=4.48 µm median cilia length)

Journal of Cell Science (2018) 131, jcs218487. doi:10.1242/jcs.218487

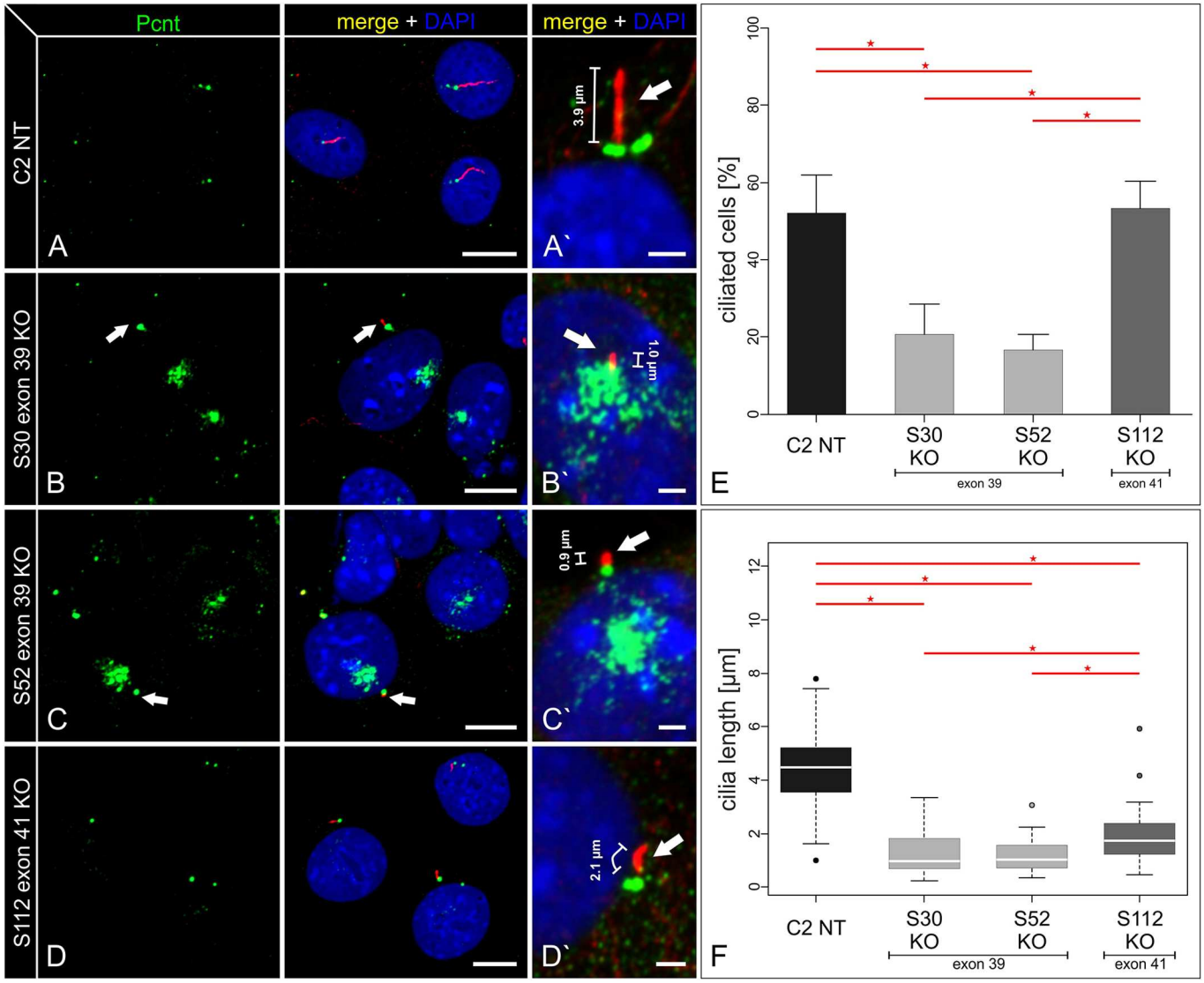

Fig. 6. Number of primary cilia and cilia length in Syne-2-depleted cells compared with non-target WT control cells. (A-D) Immunofluorescence staining of 72 h-starved mIMCD3 cell lines C2 NT (A, non target/WT), Syne-2 KO S30, S52 (B,C, exon 39) and S112 (D, exon 41) for Pcnt (green, BB marker) and acetylated tubulin (red, primary cilium marker) and nuclear staining (DAPI). (A′-D′) Higher-magnification views of the ciliary region. (A) C2 NT (WT) cells show 52% ciliated cells (E) with a median cilia length of 4.48 µm (F). Arrows indicate primary cilia. (B,C) Syne-2 KO cells S30 and S52 (exon 39) show a significant reduction with 17-21% ciliated cells (F, **P*<0.001, χ^2-test). The median cilia length was reduced to about 0.97 µm (S30) and 1.02 µm (S52) [E, S30, **P*=4.149×10^{-11}; S52, **P*=5.045×10^{-12} (Wilcoxon Mann-Whitney test)]. (D) Syne-2 KO cells S112 (exon 41) did not show any significant difference in cilia number compared with C2 NT (E, 53% ciliated cells, *P*=0.344, χ^2-test); however, ciliary length was also affected (F, 1.72 µm; **P*=1.053×10^{-15} (Wilcoxon Mann-Whitney test); S112 KO-S30 KO, **P*=0.007; S112 KO-S52 KO, **P*=0.0004]. *n*≥250 cells/cell line in E; data are mean±s.d. Box plots in F show 25th and 75th percentiles with median, whiskers are 5th and 95th percentiles; *n*≥50 cilia/cell line. Scale bars: 10 µm (A-D, merge), 2 µm (A′-D′).

(Fig. 6F). Noteworthy, the cilia of the S112 cell line were significantly longer than those originating from the S30 and S52 cell lines (exon 39).

In addition, immunofluorescence analysis in the Syne-2 KO cell lines S30 and S52 (exon 39) revealed a stronger Pcnt and mislocalized signal under serum-depleted (starvation, Fig. 6B-C′, Fig. 7A-B″) and normal conditions (Fig. S2C-D,C′-D′). The mitotic centrosomal localization of Pcnt seemed to be unaffected (Fig. S2C′,D′). In the Syne-2 KO clone S112 (exon 41), Pcnt localization was comparable with the non-target control. In these cell lines, the cytoskeleton was not affected (Fig. S2).

Quantification of protein levels using ‘stain-free technology’ on immunoblots of Syne-2 KO lysates (S30, S52) under starvation conditions corroborated the results from the immunofluorescence analysis, proving a higher expression of the known Pcnt splice variants in the Syne-2 exon 39 KO cell lines. The expression of Pcnt in the Syne-2 KO cell line S112 was similar to that in the non-target control (C2 NT) (Fig. 7E,F).

To show possible expression of a short truncated N-terminal version of Syne-2 in the KO cell lines (exon 1 – exon 39/41), we labeled the cell lines with an antibody against the N-terminus of Syne-2 (K56-386, Fig. 3B). Interestingly, we found diffuse staining in these cell lines under starvation conditions, compared with the typical outer nuclear envelope staining in the WT (Fig. 7A-D′). High-magnification images in Syne-2 KO cells S30 and S52 (Fig. 7A″,B″) revealed no colocalization of the truncated Syne-2 and Pcnt. In contrast, colocalization of Syne-2 and Pcnt can be detected in the Syne-2 KO S112 (truncated version including exon41) and WT cells (Fig. 7C″-D″).

Journal of Cell Science (2018) 131, jcs218487. doi:10.1242/jcs.218487

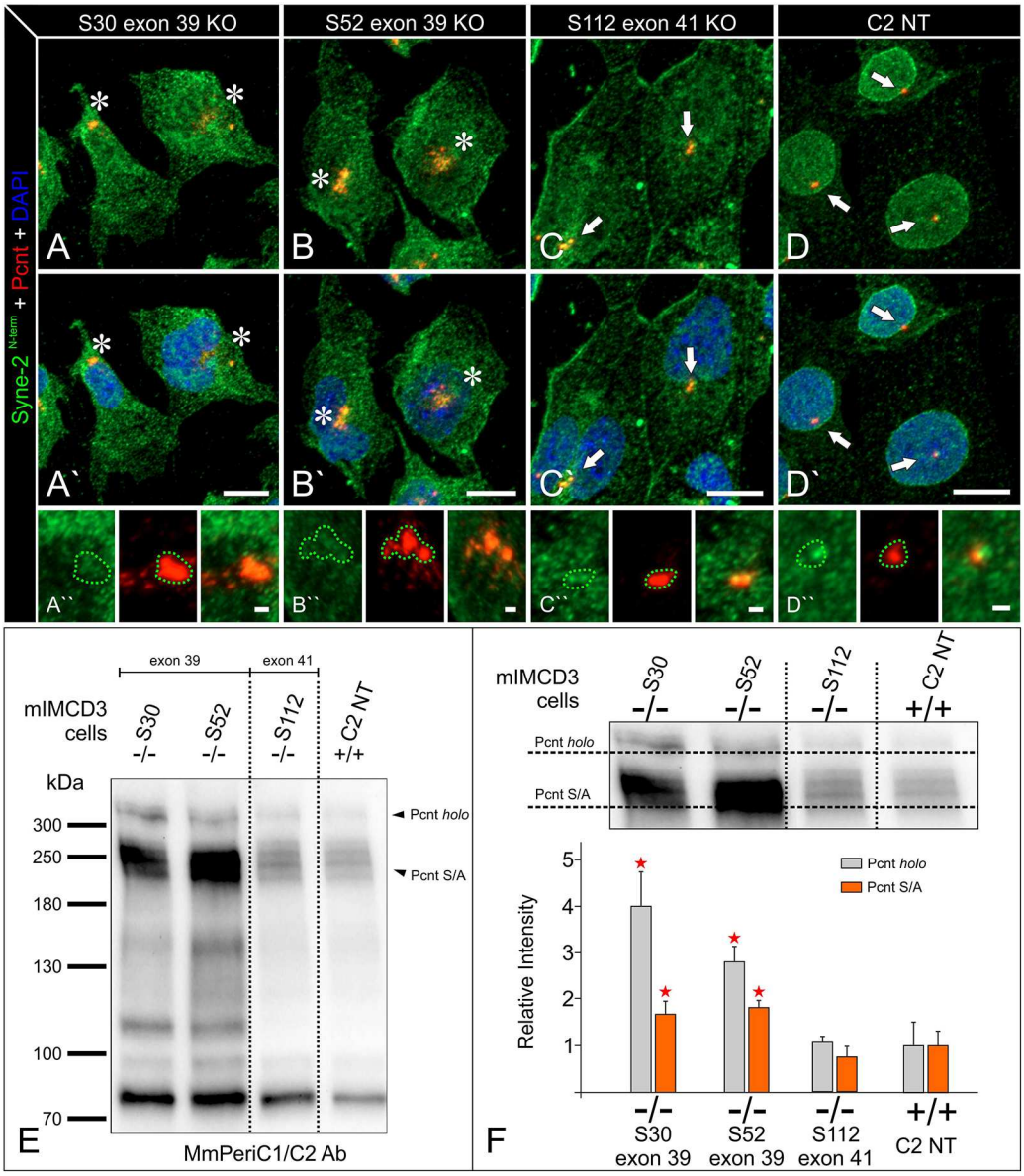

Fig. 7. Truncated Syne-2/Pcnt localization and expression in Syne-2 KO cell lines. (A-D″) Immunofluorescence staining of mIMCD3 Syne-2 KO S30, S52 (exon 39), S112 (exon 41) and C2 NT (non target/WT) under starvation conditions labeled with antibodies against Syne-2$^{N\text{-}term}$ (K56-386, green), Pcnt (red, BB marker) and nuclear marker (blue, DAPI). In the generated Syne-2 KO cells, an N-terminal truncated form of Syne-2 can be detected throughout the cytoplasm. Typical outer nuclear membrane staining is found only in WT (C2 NT) cells. The staining also reveals increased expression of Pcnt with an localization away from the centrioles in the Syne-2 KO S30 and S52 (exon 39, A-B′, asterisks), whereas centrosomal localization of Pcnt in Syne-2 KO S112 and WT (arrows) seems unaffected (C-D′). High-magnification images in Syne-2 KO cells S30 (A″) and S52 (B″) reveal no colocalization of the truncated Syne-2 and Pcnt (centrosomes in green dotted lines). In contrast, a clear colocalization in the Syne-2 KO S112 (C″) and C2 NT (D″) can be detected (centrosomes bordered in green). (E) Expression of Pcnt protein in Syne-2 KO cell lines under starvation conditions was confirmed by immunoblotting with an anti-Pcnt antibody (MmPeriC1/C2). The 360 kDa protein band is detected in these samples. A second protein band with varying molecular weight, ~230-250 kDa, suggests the expression of the different Pcnt variants A and S. (F) Micrograph of the mean band intensity measurement of the Pcnt splice variants normalized to total protein with stain-free technique (BioRad) and compared with control (C2 NT). The immunoblot (E) and the western blot analysis (F) shows that in the Syne-2 KO cell lines S30 and S52, Pcnt *holo* and the splice variants are significant higher expressed compared with non-target control (C2 NT) and S112 (**P*<0.05; data are mean±s.d.; *n*=5; Wilcoxon Mann-Whitney test). Scale bars: 5 µm (A-D″).

Since defects in primary cilia have often been observed to coincide with defects in the correct architecture of the Golgi (Gonçalves et al., 2010; Greer et al., 2014; Zahnleiter et al., 2015), we stained starved Syne-2 KO and control cells lines for Golgi structures (antibody GM130). Syne-2 KO cell lines S30 and S52 (exon 39) showed disorganized Golgi membranes and mislocalized Pcnt (Fig. S3A-B′). In the S112 Syne-2 KO (exon 41) cell line, the Golgi membranes also seemed disorganized, but Pcnt still localized to the basal body complex (Fig. S3C,C′). The control cells (C2 NT) showed the typical compact arrangement of Golgi stacks close to the nucleus and organization around the basal body complex (Fig. S3D,D′).

In summary, in the mIMCD3 KO cell lines S30 and S52 (exon 39) with a deletion of the Pcnt binding site in Syne-2, ciliogenesis and the localization and expression of Pcnt were altered. In contrast, in the mIMCD3 KO cell line S112 (exon 41), where the Pcnt binding site in Syne-2 is still present, cilia length but not cilia number was affected,

Journal of Cell Science (2018) 131, jcs218487. doi:10.1242/jcs.218487

and Pcnt expression and localization was unaltered. In the Syne-2 KO cell lines, Golgi membranes were disorganized.

DISCUSSION

Pcnt is a highly conserved protein of the pericentriolar material that adopts fundamental functions at the centrosome and base of cilia. The association of Pcnt with diseases such as MOPD II (microcephalic osteodysplastic primordial dwarfism type 2; Rauch et al., 2008; Willems et al., 2010), cancer, neuronal disorders and various ciliopathies (Delaval and Doxsey, 2010) underlines the necessity for a deeper cell biological understanding of the function of Pcnt. In the present study, we examined the function of Pcnt in photoreceptors of mouse retina.

Pcnt is required for photoreceptor development

As we previously showed, Pcnt localizes to the basal body complex of photoreceptor sensory cilia in mouse retina (Mühlhans et al., 2011). To study Pcnt function in photoreceptors, we choose a shRNA-based knockdown approach. Knockdown of Pcnt in mouse fibroblasts caused cell-cycle arrests in G1 phase, multiple cell nuclei and often, more than two centrosomes (Fig. 1), comparable to results previously described for human cell lines (Srsen et al., 2006; Graser et al., 2007; Mikule et al., 2007; Chen et al., 2014). In addition, knockdown of Pcnt in murine IMCD3 cells inhibited primary cilia assembly after induction of ciliogenesis by serum depletion (Fig. 1G), confirming the observations in human hTERT RPE1 cells (Jurczyk et al., 2004). Knockdown of Pcnt in mouse retina resulted in a disorganized retina structure, mislocalized cell nuclei in the outer retina, and defects in connecting cilia and OS formation (Fig. 2). The observed phenotype suggests a role of Pcnt in retinal development by regulating photoreceptor ciliogenesis and OS formation.

Syne-2 interacts with Pcnt

To gain insight into ciliary mechanisms associated with ciliogenesis and OS formation, we screened for binary Pcnt interaction partners using an interaction trap screen in yeast (Y2H) and a retinal mouse cDNA library. In addition, we purified the subunits of the Pcnt-associated protein complex in HEK293T cells (tandem affinity purification system). We identified a group of Pcnt interaction partners with known functions at/in the nucleus (Fig. 3C), among which was Syne-2, a large 800 kDa protein (Fig. 3B,C). Syne-2, alternatively known as nesprin-2 and NUANCE, belongs to the nuclear envelope spectrin-repeat protein family (nesprins). To date, four separate Syne genes have been identified in vertebrates (*Syne1* to *Syne4*), which give rise to a multitude of structurally and functionally diverse splice variants (Lu et al., 2012; for a review, see Rajgor and Shanahan, 2013). Syne-2 is a known mediator of nuclear migration and positioning during retinal development in flies, zebrafish and mice (Patterson et al., 2004; Tsujikawa et al., 2007; Yu et al., 2011), and Syne-2 depletion was shown to be involved in retinal degeneration and ciliogenesis in general (Dawe et al., 2009; Yu et al., 2011). These data indicate a potential functional interaction with Pcnt. We validated the interaction between Syne-2 and Pcnt and specified the Pcnt binding epitope of Syne-2 to aa residues 1921-2066 (Fig. 3).

Our immunocytochemical results showed that the subcellular localization of Syne-2 in the murine retina is confined to the IS of photoreceptors and partially overlaps with the BBC of the cilium (Fig. 4). Here, we also investigated the localization of Pcnt (Mühlhans et al., 2011). To determine whether both proteins directly interact under more native conditions, we performed *in situ* proximity ligation assays (PLAs) (Gustafsdottir et al., 2005; Söderberg et al., 2006) on vertical retinal sections of WT mice. Distinct PLA signals at the ciliary region of photoreceptors validated the direct interaction of the two proteins at the basal body complex in photoreceptors (Fig. 4D,E).

Deletion of the Pcnt-interacting domain from Syne-2 affects ciliogenesis

In cultured mammalian cells, Syne-2 splice variants lacking the KASH domain have been implicated in ciliogenesis via interaction with the transmembrane proteins meckelin and MKS1. Transient siRNA-based downregulation of either Syne-2 or meckelin results in a decrease of cilia formation (Dawe et al., 2007, 2009). To study the potential role of Syne-2 in primary cilia formation, we used the CRISPR/Cas9 system, which allows the introduction of biallelic loss-of-function effects. Syne-2 depletion affected ciliogenesis in non-cycling mIMCD3 cells in two out of the three generated KO clones (Fig. 6). While the percentage of ciliated cells after 72 h starvation was significantly reduced in the Syne-2 KO cell lines of exon 39 (S30 and S52), the KO cell line of exon 41 (S112) showed no alterations in the percentage of ciliated cells compared with non-targeted WT cell lines (Fig. 6E). Ciliary length was significantly reduced in the Syne-2 KO cell lines compared with non-targeted WT lines, albeit to a lesser extent in cell line S112 (Fig. 6F). These differences can be explained by either residual activity of truncated expressed Syne-2 protein, or by the requirement of the Pcnt interaction domain of Syne-2 for ciliogenesis and cilium length control, which is deleted only in the exon 39 KO cell lines (Fig. 7A-D″). The latter is supported by the altered localization of Pcnt away from the basal body complex and the overexpression of Pcnt found in the exon 39 KO cell lines (Figs 6B-C′ and Fig. 7, Figs S2, S3). The reduced ciliary length in cell line S112 may indicate that additional interaction domains with other proteins controlling ciliary length, expressed after exon 41 in WT Syne-2, are deleted in cell line S112 (Avasthi and Marshall, 2012; Wheway et al., 2015). Interestingly, the mutation in exon 39 of Syne-2 not only mislocalized Pcnt to the Golgi membrane, but also altered the shape of the Golgi. It is known that cells with mutated or knocked down ciliary proteins show a disorganized Golgi, which makes the Golgi an extraciliary site for ciliary proteins (Gonçalves et al., 2010; Dafinger et al., 2011; Zahnleiter et al., 2015).

Pcnt contains two Syne-2 binding sites

Our study provides evidence that Pcnt contains two binding sites for Syne-2, one at the N-terminus and one at the C-terminus. We propose that this could be attributed to a development-dependent expression of Pcnt splice variants in the retina. Adult mouse photoreceptors express predominantly one of the smaller *Pcnt* splice variants, most likely encoding the variant Pcnt S, which lacks the N-terminal domain (Fig. 1A). The larger Pcnt B splice variant is strongly expressed in retinal cells other than photoreceptors (Mühlhans and Gießl, 2012). The cell type-specific allocation of Pcnt splice variants in the adult retina suggests that the C-terminal Syne-2 binding site is present in Pcnt part 5 (see Fig. 3A). The distinct expression pattern of Pcnt in mouse retina development is not yet known. However, Zebrowski and colleagues investigated Pcnt expression in rat heart development showing that Pcnt B is ubiquitously expressed at the examined developmental stages. In contrast, expression of Pcnt S appeared shortly before birth in the heart (Zebrowski et al., 2015). Assuming a similar Pcnt expression pattern in retinal development, the interaction of Pcnt and Syne-2 could be mediated via the N-terminal binding site present in Pcnt part 2 (Fig. 3A).

Journal of Cell Science (2018) 131, jcs218487. doi:10.1242/jcs.218487

Based on the results of our study, we propose two spatio-temporally separated roles of the interaction of Pcnt and Syne-2 in mouse photoreceptors (Fig. 8).

Proposed function 1: role of Pcnt and Syne-2 in ciliogenesis

The formation of cilia is initiated by the migration of the centrosome to the apical cell surface in a microtubule-dependent manner (Dawe et al., 2007; Adams et al., 2008). According to Dawe and colleagues, Syne-2 seems to be required for proper centrosome migration prior to ciliogenesis (Dawe et al., 2009). The physical centrosome-cytoskeletal connection, which regulates centrosome position at the beginning of ciliogenesis, could be provided by an interaction of Pcnt and Syne-2. This interaction is lost in our CRISPR/Cas9 experiments targeting exon 39, leading to a reduction in cilia number and shorter cilia (Fig. 8B). In contrast, the CRISPR/Cas9-mediated mutation in exon 41, which leads to a truncated Syne-2 protein that still includes the Pcnt interaction domain, has no effect on cilia number, but only on ciliary length (Fig. 8C).

Proposed function 2: role of Pcnt and Syne-2 in nucleus attachment to the centrosome

Syne-2 is critical during nuclear migration, which is necessary for proper retinal development (Patterson et al., 2004; Kracklauer et al., 2007; Tsujikawa et al., 2007; del Bene et al., 2008; Yu et al., 2011). Our Pcnt siRNA data revealed a phenotype similar to the KASH-domain-deleted Syne-2 mouse (Syne-2^{tm1Rexu}, MGI) with mislocalized cell nuclei in the photoreceptor cell layer, indicating that Pcnt is important for nuclear positioning in the retina. Neuronal cell migration is initiated by the extension of a leading process in the direction of migration, whereupon microtubules extend anteriorly into the leading process. Owing to the movement of cytoplasmic dynein towards the minus-ends of microtubules, the centrosome is positioned in the leading process in front of the nucleus. Next, the

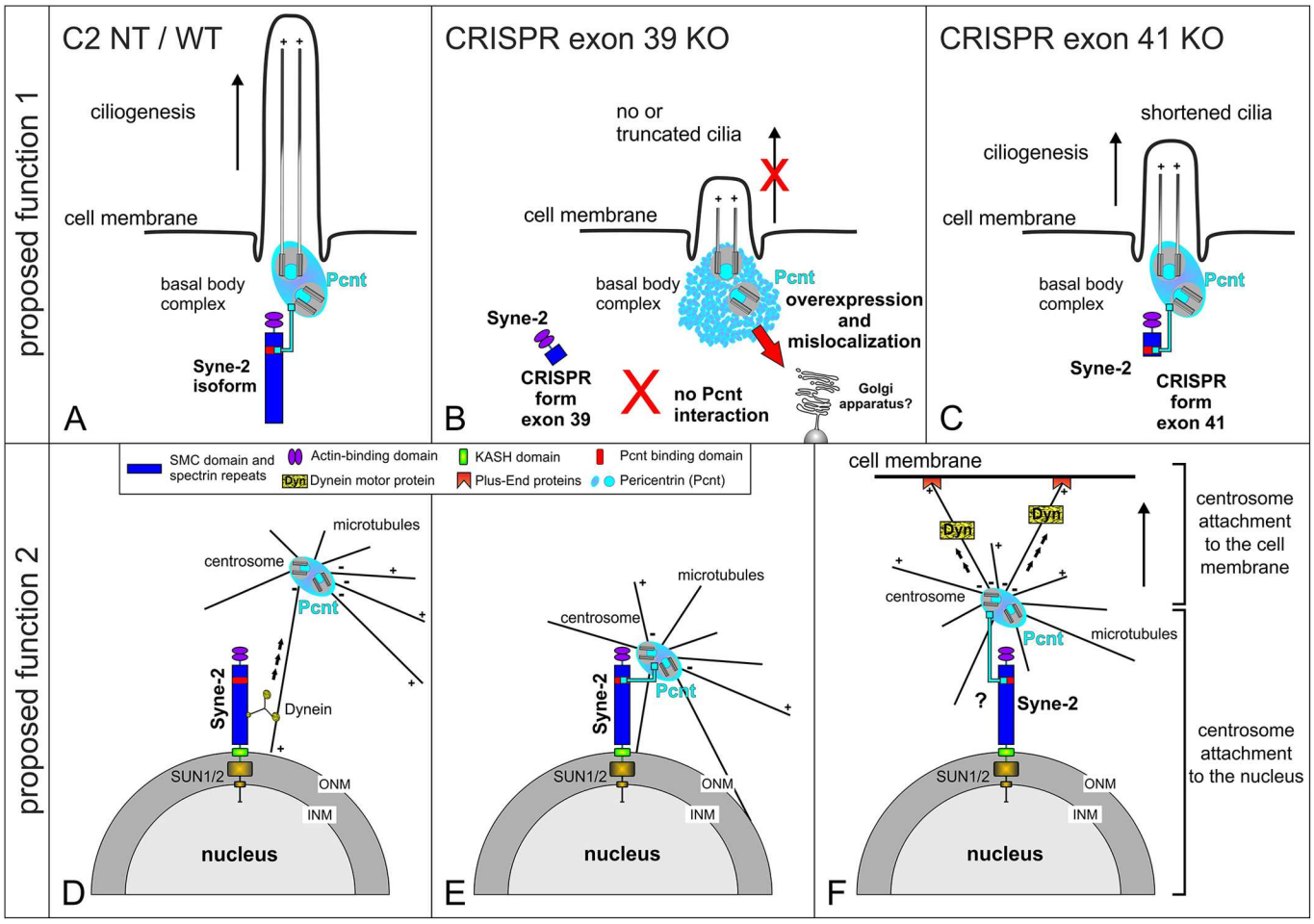

Fig. 8. Two different proposed functional roles for the interaction of Pcnt and Syne-2 isoforms, and their possible effects in ciliogenesis and nuclear attachment to the centrosome. (A-C) Proposed function 1: recapitulation of our findings in ciliogenesis of primary cilia in mIMCD3 cells. (A) Our results revealed that KASH-domain-lacking isoforms of Syne-2 are directly involved in ciliogenesis. A deletion of the Pcnt binding domain in Syne-2 (B, exon 39 CRISPR KO) results in the formation of no cilia or truncated cilia. Additionally, these cells show an overexpression and mislocalization of Pcnt to the Golgi membranes. Knockout of Syne-2 in C-terminal regions with respect to the Pcnt-interaction-domain (C, exon 41 CRISPR KO) does not affect ciliogenesis, but results in a significant reduction of ciliary length compared with WT. (D-F) Proposed function 2: The KASH protein Syne-2 is localized in the outer nuclear membrane (ONM) and is able to bind cytoplasmic dynein, mediating the attachment of the nucleus to microtubules (D). As dynein translocates toward the minus-end of microtubules, the nucleus and the centrosome come in close proximity. (E) Pcnt is an integral part of the pericentriolar material surrounding the centrosome. Assuming an interaction between Pcnt and Syne-2, both proteins may directly organize the attachment of the nucleus to the centrosome. (F) The attachment of both organelles plays an important role in nuclear as well as neuronal migration. Movement of the nucleus is achieved by the preceding centrosome, which is pulled in a dynein-dependent manner toward microtubules anchored by plus-end proteins in the cell membrane. As nuclear migration is a key feature of retinogenesis, Pcnt and Syne-2 seem to be essentially involved in mammalian retinal development. INM, inner nuclear membrane.

nucleus is pulled towards the centrosome and the trailing cell body follows the nucleus to achieve the appropriate laminar position. Consequently, the attachment of the nucleus to the centrosome is critical for nuclear translocation (nucleokinesis) within neuronal migration (Morris, 2003; Tsai and Gleeson, 2005; Zhang et al., 2009). Yu and colleagues were able to confirm that the outer nuclear membrane protein Syne-2 interacts with the motor protein complexes of cytoplasmic dynein or dynactin and kinesin. This interaction mediates the coupling between the nucleus and the microtubule cytoskeleton during nuclear migration (Yu et al., 2011). Similar mechanisms have also been shown in *Drosophila* and Zebrafish retinas (Patterson et al., 2004; Kracklauer et al., 2007; Tsujikawa et al., 2007; del Bene et al., 2008). The physical link between the nucleus and the centrosome could be controlled by the interaction of a nucleus-associated KASH protein and a component of the pericentriolar material (Malone et al., 2003). In *C. elegans*, the proximity of the centrosome and nucleus is established by the KASH domain protein ZYG-12 in the nuclear envelope and the dynein light intermediate chain 1 (DLI-1) (Malone et al., 2003). From the comparable cellular localization of Pcnt and Syne-2 in mice, we suggest that the interaction of the two proteins (verified in this study) plays a role in the association of the nucleus to the centrosome. Here, we showed that in mice, Pcnt acts as the centrosomal component, whereas Syne-2 takes over the nucleus-anchoring part. Together, Pcnt and Syne-2 form the nucleus-centrosome complex (Fig. 8D-F). Consequently, Pcnt and Syne-2 seem to be essential components of the mechanism of nuclear migration in the mammalian retina. It has already been shown that Pcm1 and Disc1, both centrosome-localized Pcnt-interacting proteins, are involved in neuronal migration in the developing cerebral cortex (Kamiya et al., 2008; Delaval and Doxsey, 2010). Our findings are also consistent with a recently published study, in which Pcm1, Pcnt and other centrosomal proteins are shown to be anchored to the nuclear envelope by Syne-1 in differentiating mouse myoblasts (Pcm1 and Syne-1 were also identified in our Pcnt-TAP screen; Fig. 3C) (Espigat-Georger et al., 2016).

Taken together, the interaction between Pcnt and Syne-2 is required for ciliogenesis and ciliary length control, and seems to play a role in centrosomal-mediated nuclear migration.

MATERIALS AND METHODS

Ethics statement

The experiments were performed in compliance with the guidelines for the welfare of experimental animals issued by the Federal Government of Germany and the University of Erlangen-Nuremberg. The animal experiments were approved and registered by the local authorities (Regierung von Mittelfranken, AZ54-2531.31-26/07; Amt für Veterinärwesen der Stadt Erlangen, AZ TS-10/07 Lehrstuhl für Zoologie-Tierphysiologie). Mouse breeding was performed in the animal facilities of the University of Erlangen-Nuremberg according to European and German laws on experimental animal welfare (Tierschutzgesetz; AZ820-8791.2.63).

Animals

Adult C57BL/6J mice (age 2-4 months) of either sex were used in this study. The animals were kept in a 12 h:12 h light:dark cycle with lights on at 06:00 h and with food and water *ad libitum*.

Mouse Pcnt splice variants

The nomenclature in NCBI is highly confusing. We prefer to refer to the Pcnt splice variants Pcnt A, B and S, because they are well described in the literature (e.g. Miyoshi et al., 2006a; Endoh-Yamagami et al., 2010). The sequence of Pcnt A (AN: partial, AAO24322.1) stated in NCBI represents just the C-terminal part of Pcnt A, as the N-terminal part remains the same as in the full-length mRNA. Pcnt isoforms X1-X14 are predicted by automated computational analysis and have not yet been validated.

Tandem affinity purification

HEK293T (human embryonic kidney) cells were transfected with constructs that encoded Pcnt parts 1 to 5 fused to an SF-TAP tag (Gloeckner et al., 2007) as described in the Cell culture section below. After 48 h, transfected cells were lysed in lysis buffer containing 30 mM Tris-HCl (pH 7.4), 150 mM NaCl, 0.5% Nonidet-P40, protease inhibitor cocktail (Roche Diagnostics, Mannheim, Germany) and phosphatase inhibitor cocktail 1 and 2 (Sigma-Aldrich, Taufkirchen, Germany) for 20 min at 4°C. After sedimentation for 10 min at 10,000 ***g***, the cleared supernatant was incubated for 1 h at 4°C with Strep-Tactin superflow beads (IBA, Göttingen, Germany). Subsequently, the resin was washed three times in wash buffer (30 mM Tris-HCl, pH 7.4, 150 mM NaCl, 0.1% Nonidet-P40) supplemented with phosphatase inhibitors. Protein complexes were eluted with 2 mM desthiobiotin (IBA) in TBS. For the second purification step, the eluates were transferred to anti-FLAG M2 agarose beads (Sigma-Aldrich) and incubated for 1 h at 4°C. The FLAG beads were washed three times with wash buffer and proteins were eluted with FLAG peptide (200 µg/ml, Sigma-Aldrich) in TBS. 5% of the sample was separated by SDS-PAGE and proteins were stained with silver according to standard protocols. The remainder of the protein sample was precipitated with chloroform and methanol. Protein precipitates were stored at −80°C.

Mass spectrometry

Mass spectrometric analyses were performed as described (Boldt et al., 2016). Following precipitation, SF-TAP-purified complexes were solubilized and proteolytically cleaved using trypsin. The resulting peptide samples were desalted and purified using stage tips before separation on a Dionex RSLC system. Eluting peptides were directly ionized by nano-spray ionization and detected by a LTQ Orbitrap Velos mass spectrometer (Thermo Fisher Scientific, Waltham, USA). Mascot was used to search the raw spectra against the human SwissProt database for identification of proteins. The Mascot results were verified by Scaffold (version Scaffold 4.02.01, Proteome Software Inc., Portland, OR, USA) to validate MS/MS-based peptide and protein identifications.

Yeast two-hybrid analysis

For yeast two-hybrid analysis, Pcnt parts 1 to 5 were fused to a DNA-binding domain (GAL4-BD) and used as baits to screen a murine retinal cDNA library. Bait plasmids, carrying the *HIS3* (histidine), *ADE2* (adenine), *MEL1* (α-galactosidase) and *lacZ* (β-galactosidase) reporter genes, were used to transform the *S. cerevisiae* strain AH109. A murine retina cDNA library was generated according to manufacturer's instructions ('Mate&Plate' Library System, Clontech, Mountain View, CA, USA), cloned into pGADT7 vectors and transformed into the *S. cerevisiae* strain Y187. Yeast techniques and two-hybrid methods were performed according to the Yeast Protocols Handbook and the Matchmaker GAL4 Two-Hybrid System 3 manual (Clontech). Interactions were assessed by auxotrophic and colorimetric selection markers corresponding to the activation of the yeast reporter genes (*HIS*, *ADE*, *lacZ*). To amplify the cDNA of the positive clones, a small sample of a yeast colony was collected using a pipette tip and a colony PCR was performed using primers specific for the prey plasmid. PCR products were then purified by the Agencourt CleanSeq Kit (Beckman Coulter, Krefeld, Germany) and sequenced using the BigDye terminator reagent v.3.1 (Applied Biosystems, Life Technology, Foster City, CA, USA). Capillary electrophoresis was performed using the ABI 3730 sequencer (Applied Biosystems) and electropherograms were analyzed using Chromas 2 (Chromas MFC Application, Technelysium Pty Ltd, South Brisbane, Australia) and SeqMan II (DNASTAR Inc., Madison, WI, USA). The identity of the proteins corresponding to the DNA sequences of the single yeast clones was identified by BLAST (https://blast.ncbi.nlm.nih.gov/Blast.cgi) and BLAT (http://genome.ucsc.edu/cgi-bin/hgBlat) analysis.

Binary yeast two-hybrid assay (1-on-1 assay)

Interaction between Pcnt part 2/5 and Syne-2 was confirmed via an α-galactosidase assay. The strength of the interaction was quantified by performing a β-galactosidase liquid culture assay (Croci et al., 2003).

Therefore Pcnt constructs were cloned into the pGADT7 vector and transformed in *S. cerevisiae* strain Y187. A murine Syne-2 construct (1852-2143 aa; NM_001005510.2) was cloned into the pGBKT7 vector and transformed in *S. cerevisiae* strain AH109. Colorimetric assays were carried out according to the Yeast Protocols Handbook (Clontech) and (Croci et al., 2003). As a positive control, the well-known interaction between the SV40 large T antigen (SV40-TA) and the tumor suppressor protein p53 (Matchmaker Gal4 Two-Hybrid System 3, Clontech) and as a negative control the SV40 large T antigen (SV40-TA) and Syne-2 in pGBKT7 was used.

GST pull-down assays

A Syne-2 fragment (1921-2066 aa; NM_001005510.2) was cloned into the pDEST15 vector (Gateway cloning system, Invitrogen) encoding the Glutathione S-transferase affinity tag at the N-terminus. For the creation of GST-fusion proteins, *Escherichia coli* BL21-AI cells were transformed with pDEST15 constructs. Bacterial cultures were induced with 0.2% arabinose at 37°C, and then harvested by centrifugation at 4000 ***g*** for 15 min at 4°C. Cell pellets were lysed with lysozyme solution (Sigma-Aldrich, Taufkirchen, Germany) in PBS on ice for 30 min. Afterwards lysates were treated with ultrasound and centrifuged at 16,000 ***g*** for 25 min at 4°C. Glutathione Sepharose 4B beads (GE Healthcare, Munich, Germany) were used to bind the GST fusion proteins from the supernatant. For this purpose, 1 ml GST-Syne-$2^{1921\text{-}2066}$ fusion protein was added to the beads and incubated for 3 h at 4°C. After incubation, beads were washed with HNTG buffer (10% Glycerol, 0.1% Triton X-100, 20 mM HEPES, 120 mM NaCl, 1 mM $CaCl_2$, pH 7.5). GST protein-coated beads were incubated at 4°C overnight with HEK293T cell lysates expressing SF-TAP-tagged Pcnt-part 2 or Pcnt-part 5. After incubation, beads with bound protein complexes were washed in HNTG buffer. Then beads were taken up in Laemmli sample buffer and heated for 5 min at 75°C. The presence of SF-TAP-tagged Pcnt part 2/5 in complex with GST-Syne-$2^{1921\text{-}2066}$ was assessed by immunoblotting using an anti-FLAG M2 antibody (Sigma-Aldrich, Taufkirchen, Germany).

Cell culture

All cell lines were obtained from American Type Culture Collection American Type Culture Collection (Wesel, Germany) and were tested every month for contaminations. For tandem affinity purifications HEK293T cells were grown in DMEM (Life Technologies, Carlsbad, CA, USA) supplemented with 10% fetal bovine serum. Cells were seeded, grown overnight and then transfected with the SF-TAP-tagged Pcnt constructs using JetPei (Polyplus transfection, Illkirch-Graffenstaden, France) according to the manufacturer's instructions. Forty-eight hours later, cells were processed as described in the Tandem affinity purification section.

For GST pull down assays (HEK293T) and western blotting (Syne-2 CRISPR) cells were washed in PBS and lysed on ice in extraction lysis buffer (50 mM Tris-HCl, pH 7.5, 150 mM NaCl, 1% Triton X-100, 0.5% sodium deoxycholate) supplemented with protease inhibitor cocktail (Roche, Basel, Switzerland). Lysates were treated with ultrasound and centrifuged at 16,000 ***g*** for 15 min at 4°C. Samples were taken from the supernatant to estimate total protein concentration.

Ciliogenesis (in 3T3 mouse fibroblasts and mIMCD3 mouse kidney cells) was induced by incubating cells in serum-free medium (DMEM 0% FBS, 1:1 diluted with PBS) for a period of 3 days. Cells were fixed as described in 'Immunofluorescence microscopy' and stained with ciliary marker (acetylated tubulin, polyglutamylated tubulin) and centrosomal marker (γ-tubulin, pericentrin). Cilia measurements were madeon the basis of the fluorescence images (*z*-stacks; 63× magnification). The measurement was carried out in triplicates using the ZEN blue 2012 software.

Quantitative PCR

Quantitative PCR analyses were performed as described (Regus-Leidig et al., 2014). Total RNA from shRNA treated cells was isolated using the RNeasy Kit (Qiagen) and subjected to reverse transcription using the iScript™cDNA Synthesis Kit (Bio-Rad, Munich, Germany) in a total volume of 20 µl. For quantitative PCR, 1 µl of cDNA was used in a total volume of 12.5 µl containing 6.25 µl of 2× Sso Fast Eva Green Supermix (Bio-Rad) and 160 nM of target gene forward and reverse primer. Amplification was carried out in a CFX 96 Real-Time PCR Detection System (Bio-Rad). The relative expression of the known *Pcnt* isoforms, normalized to *Actb*, *Pbgd* and *Gapdh*, was calculated using the Bio-Rad CFX Manager 3.1 software (Bio-Rad). The following primer sets were used (5′ to 3′): Pcnt: Forward primer1: GTCAGTTCATGGATGATC; Reverse primer1: TTTTTCTCTCAGTTTTTCTT, Forward primer2: GGAGCAGGAAAAGTGATG; Reverse primer2: GTGACTGGACAAACCTTC; β-actin: Forward primer: ATGCTCCCCGGGCTGTAT; Reverse primer: TCACCCACATAGGAGTCCTTCTG; GAPDH: Forward primer: CAACTTTGTCAAGCTCATT; Reverse primer: TCTGGGATGGAAATTGTG; PBGD: Forward primer: ACAAGATTCTTGATACTGCACTCTCTAAG; Reverse primer: CCTTCAGGGAGTGAACGACCA. Negative controls were treated as above without adding template and amplicon sizes were verified on 1% agarose gels stained with ethidium bromide (Roth, Karlsruhe, Germany).

CRISPR/Cas9 genome editing

For CRISPR experiments, mIMCD3 cells were cultured using DMEM (Life Technologies, Carlsbad, CA, USA). Supplements were 0-10% fetal bovine serum depending on the experiment and 1% antibiotic mixture (penicillin-streptomycin). Cells were seeded, grown overnight and then transfected with the Syne-2 CRISPR (Sigma-Aldrich, vector pVAX-Cas9 Nuclease and CRISPR06 Sigma Universal Negativ Control 1, Table S1) constructs using PEI. After 2 days of incubation, GFP-positive cells were sorted into 96-well plates via FACS. Genomic DNA was isolated with the DNeasy Blood & Tissue Kits (Qiagen) according to the manufacturer's instructions. PCR Cycling conditions were 35 cycles at 94°C for 45 s, 60°C for 30 s and 72°C for 1 min 40 s followed by a 10 min 72°C extension step. Primers specific for Syne-2 CRISPR region: forward primer exon 39 (5′-AGTCTCACATTCGGATTGCCAG-3′), reverse primer exon 39 (5′-AGTATGCACTGACTGTCTCAGC-3′), forward primer exon 41 (5′-ATTTGGGAGTGTGCTTTCTCCG-3′), reverse primer exon 41 (5′-ATTGCCCTCTTGGAAGAGGAG-3′). PCR products were purified by the Agencourt CleanSeq Kit (Beckman Coulter, Krefeld, Germany) and sequenced using the BigDye terminator reagent v.3.1 (Applied Biosystems, Life Technology, Foster City, CA, USA). Capillary electrophoresis was performed using the ABI 3730 sequencer (Applied Biosystems) and electropherograms were analyzed using Chromas 2 (Chromas MFC Application, Technelysium Pty Ltd, South Brisbane, Australia) and SeqMan II (DNASTAR Inc., Madison, WI, USA). Nucleotide numbering uses +1 as the A of the ATG translation initiation codon in the reference sequence (NM_001005510.2), with the initiation codon as codon 1.

Western blot analysis

Western blot analysis was performed as described (Mühlhans et al., 2011). Briefly, proteins were separated by SDS-PAGE using 10% polyacrylamide gels, 3-8% NuPAGE Novex Tris-Acetate Gels (Life Technologies) or 4-15% Mini-PROTEAN TGX Stain-Free (Bio-Rad Laboratories, Munich, Germany). Blotting was perfomed in a semi-dry blot chamber (Trans-Blot Turbo Transfer System, Bio-Rad Laboratories) by 25 V for 30-40 min at room temperature (RT) to polyvinylidene difluoride (PVDF) membranes (Amersham Hybond- P, GE Healthcare or Transblot Turbo Midi-size LF PVDF membranes, Bio-Rad Laboratories). Membrane was blocked 1 h with blocking solution (0.2% Applichem Blocking Reagent, 10 mM Tris-HCl, 150 mM NaCl, pH 7.4) and probed with primary antibodies and horseradish peroxidase-labeled secondary antibodies. Imaging and quantification (mean band intensity measurement normalized to total protein with stain-free technique) were performed with a molecular imager, 'Stain-free technology' and the Image Lab software (ChemiDoc XRS; Bio-Rad Laboratories). Protein separation can be visualized on the gel after electrophoresis. Protein transfer to the membrane can be confirmed and assessed prior to blot detection, and blot normalization can occur without the extra steps required for typical reference protein detection.

Immunofluorescence microscopy

Preparation of retinal tissue and antibody incubation for light microscopic immunocytochemistry were performed as described previously (Mühlhans et al., 2011). Sections were incubated with 0.01% Tween 20 in PBS for 10 min and washed for 15 min in PBS. Next, samples were blocked for 45 min in blocking solution (0.5% cold-water fish gelatin and 0.1%

Journal of Cell Science (2018) 131, jcs218487. doi:10.1242/jcs.218487

ovalbumin in PBS), followed by overnight incubation with primary antibodies diluted in blocking solution at 4°C. On the following day, the samples were washed 3× for 10 min with PBS and incubated with secondary antibodies in blocking solution with DAPI (4,6-diamidino-2-phenylindole) (1:50,000, Sigma-Aldrich). After additional 3×10 min PBS washing steps, samples were mounted in Aqua Poly Mount (Polysciences, Eppelheim, Germany) and analyzed with a Zeiss Axio Imager Z2 equipped with an ApoTome by using ZEN blue 2012 software or imaged on a Laser Scanning Microscope 710 by using ZEN black 2010 software with corresponding imaging modules (Zeiss, Oberkochen, Germany). Images were adjusted for contrast and brightness using Adobe Photoshop CS6 (Adobe Systems, San Jose, CA, USA) and figures were arranged using Corel Draw X8 (Corel GmbH, Munich, Germany). In order to study three-dimensional (3D) protein distributions, *z*-stacks were taken (stack interval: 0.193-0.195 µm) and fused to 3D images using Imaris 7.6 (Bitplane).

Antibodies

For immunocytochemistry on cryostat sections (ICC) and western blotting (WB), the following antibodies were used: rabbit anti-Pcnt MmPeriC1/C2 pAb (ICC 1:500, WB 1:250) as previously described (Mühlhans et al., 2011); mouse anti-Flag M2 mAb (WB 1:3000, #F1804), mouse anti-Opsin mAb clone RET-P1 (ICC 1:40,000, #O4886), mouse anti-α-tubulin mAb clone DM1A (ICC 1:700, #T9026), mouse anti-acetylated tubulin 6-11B-1 (ICC 1:1000, #T7451) (all from Sigma-Aldrich); mouse anti Syne-2 F-11 mAb (ICC 1:100, WB 1:250, #sc-398616), rabbit anti-PCM1 pAb (ICC 1:700, #sc-67204) (both Santa Cruz Biotechnology, Santa Cruz, CA, USA); rabbit anti-PC2 pAb (ICC 1:100, #AB9088; Millipore GmbH Schwalbach/Ts, Germany); mouse anti-Piccolo (ICC 1:1000; #142111, Synaptic Systems, Göttingen, Germany); mouse anti-polyglutamylated tubulin GT335 (ICC 1:1000; #AG-20B-0020, Biomol, Hamburg, Germany); rabbit anti-GFP (ICC1:2000; pre-EM 1:100,000, #A11122, Life Technologies, Carlsbad, CA, USA), rabbit anti-ubMunc13-2 (ICC 1:6000) as previously described (Cooper et al., 2012); guinea-pig anti-GFP (ICC 1:300) as previously described (Regus-Leidig et al., 2014); mouse anti-Syne-2 K56-386 mAb (ICC 2:1) was a gift from Angelika A. Noegel (Center for Biochemistry, Medical Faculty, University of Cologne, Germany) as previously described (Lüke et al., 2008); mouse anti-GM-130 mAb 35/GM130 (ICC 1:50, #610822, BD Bioscience, Heidelberg, Germany).

The following secondary antibodies were used: Alexa Fluor 568 and Alexa Fluor 488 goat anti-mouse, goat anti-rabbit and goat anti guinea pig IgG conjugates (1:500; Molecular Probes, Eugene, OR, USA); HRP goat anti-mouse/rabbit IgG conjugate (1:10,000; Sigma-Aldrich).

Electron microscopy

For conventional electron microscopy and good tissue preservation, retinas were fixed in 4% paraformaldehyde (PFA) and 2.5% glutaraldehyde for 2 h at RT. Tissue contrasting was carried out by incubation in 1.5% potassium ferrocyanide and 2% osmium tetroxide in 0.1 M cacodylate buffer (pH 7.4) for 1.5 h. Retinas were dehydrated using an ethanol series and propylene oxide with 0.5% uranyl acetate added at the 70% ethanol step. The tissue was embedded in RenLam resin (Serva, Heidelberg, Germany).

For pre-embedding immunoelectron microscopy, the subretinal injected retinas were prepared and stained as described previously (Mühlhans et al., 2011). Briefly, the dissected retinas were pre-fixed in 4% PFA for 50 min at RT. After four cycles of freezing and thawing, retinas were washed in phosphate-buffered saline (PBS, pH 7.4) and embedded in buffered 4% Sieve 3:1 Agarose (Biozym). Agar blocks were sectioned at a thickness of ∼100 µm with a Vibratome (Leica VT 1000S, Leica, Wetzlar, Germany). Vibratome sections were blocked in 10% normal goat serum and 1% bovine serum albumin in PBS for 2 h at RT and then incubated with appropriate primary antibodies for 4 days at 4°C. After washing the retina in PBS four times, the sections were subjected to corresponding biotinylated secondary antibodies and a peroxidase-based enzymatic detection system (Vectastain Elite ABC kit, Vector Laboratories). For immunocomplex visualization, 0.01% hydrogen peroxide (Sigma-Aldrich) was added to a 0.05% 3.3′ diaminobenzidine solution and staining was fixed in 2.5% glutaraldehyde (Sigma-Aldrich) in cacodylate buffer (0.1 M, pH 7.4) for 1 h at RT. Following silver intensification and dehydration, sections were flat-mounted in Epoxy Embedding Medium (Sigma-Aldrich).

After being sectioned on an ultramicrotome (Reichert Ultracut E), retina ultrathin sections (60-70 nm) were collected on Pioloform-coated copper grids and stained with uranyl acetate and lead citrate (Leica). The sections were examined and photographed with a Zeiss EM10 electron microscope (Zeiss) and a Gatan SC1000 Orius™ CCD camera (GATAN, Munich, Germany) in combination with the DigitalMicrograph™ software (GATAN, Pleasanton, CA, USA). Images were adjusted for contrast and brightness using Adobe Photoshop CS6 (Adobe Systems).

In situ proximity ligation assay (PLA)

The following PLA components were purchased from Sigma-Aldrich: Duolink PLA probe anti-rabbit PLUS, Duolink PLA probe anti-mouse MINUS and Duolink *in situ* Detection Reagent Red. PLAs were performed according to the manufacturer. In brief, 12-µm-thick cryosections were incubated overnight at room temperature with primary antibodies. Next, combinations of the PLA probes (anti-rabbit PLUS probe, anti-mouse MINUS probe, diluted in antibody dilution) were added to the sections for 1-2 h at room temperature. Ligation was performed for 30 min, followed by the amplification step for 100 min at 37°C. To verify correct antibody binding, the antibody mixture used for the PLA was tested in fluorescence staining on a different set of slices.

AAV vector production, preparation and subretinal injections

Cloning of the shRNA was performed by standard techniques. To insert the Pcnt shRNA (Table S1) into the AAV vector (backbone pAAV2.1-sc-shcontrol-CMV-eGFP-WPRE) the restriction sites *Hpa*I and *Bst*EII were used. The pAAV2.1-sc-sh3491-CMV-eGFP-WPRE, pAAV2.1-sc-sh4285-CMV-eGFP-WPRE and pAAV2.1-sc-shcontrol-CMV-eGFP-WPRE cis plasmids were used to produce self-complementary AAV8Y733F-pseudotyped AAV2 vectors expressing the shRNA under control of a mouse U6 promoter and eGFP under control of a CMV promoter according to published procedures (Koch et al., 2012; Becirovic et al., 2016). In brief, 293T cells were transfected with the *trans* plasmids pAdDeltaF6 and pAAV2/8 Y733F, and the corresponding *cis* plasmid using the calcium phosphate method. rAAV2/8 Y733F particles were harvested after 48 h followed by iodixanol-gradient purification. The 40-60% iodixanol interface was further purified and concentrated by ion exchange chromatography on a 5 ml HiTrap Q Sepharose column using an ÄKTA Basic FPLC system (GE Healthcare, Munich, Germany) according to previously described procedures, followed by further concentration using Amicon Ultra-4 Centrifugal Filter Units (Millipore, Schwalbach, Germany). Physical titers (in genome copies/ml) were determined by quantitative PCR on a LightCycler 480 (Roche Applied Science, Mannheim, Germany) using KAPPA SYBR FAST kit (Peqlab, Erlangen, Germany) and the following primer set: WPREF: 5′-AGTTGT-GGCCCGTTGTCAGG-3′ and WPRER: 5′-AGTTCCGCCGTGGCAAT-AGG-3′. For subretinal injection of the rAAV shRNA vectors, mouse pups (P5) were anesthetized by hypothermia. The prospective eyelid was numbed by application of a local anesthetic (Xylocain, Astra Zeneca GmbH, Wedel, Germany) and opened with a scalpel. The procedure of subretinal injections were described previously (Regus-Leidig et al., 2014).

Lentivirus production

Lentivirus was produced by transfecting a three-plasmid vector system comprising a shuttle plasmid with the shRNA (FUGW H1, CMV-eGFP) and two packaging plasmids (pCMV R8.9 and pHCMV VSVg) into HEK293T cells (grown in DMEM+10% fetal bovine serum and penicillin-streptomycin) as described previously (Leal-Ortiz et al., 2008). In brief, transfections were conducted on 90-100% confluent cell cultures with polyethylenimine (PEI) (Polyscience, Eppelheim, Germany) using 15 µg total DNA per 10 cm dish. 12 h after transfection, the medium was refreshed. After 72 h, the virus-containing medium was collected, passed through a 0.45 µm filter to remove cell debris and frozen at −80°C.

Lentiviral concentration by precipitation of lentiviral vectors using PEG 6000

A mixture of 15 ml of virus-containing medium, 4.25 ml of a 50% PEG 6000 solution, 1.88 ml 4 M NaCl stock solution and 3.87 ml PBS (25 ml) was stored at 4°C for 2 h and contents were mixed every 20-30 min.

The tubes were centrifuged at 7000 ***g*** for 10 min at 4°C using a fixed-angle rotor. The supernatant was discarded and the pellet was resuspended in 250 µl Tris-HCl (50 mM, pH 7.4), frozen on dry ice, and stored at −80°C.

Lentivirus treatment of organotypic retina cultures

C57/BL6J mouse pups (P0) were anesthetized by hypothermia, decapitated and eyes were prepared. Briefly, the isolated eyes were treated with 1.2 mg/ml proteinase K for 5 min at 37°C and quenched by adding Dulbecco's Modified Eagle's Medium (DMEM F-12) containing 10% fetal calf serum. After rinsing the eyes three times in serum-free culture medium, the retinas were dissected from the eye and cultured with photoreceptor side facing down in supplemented DMEM F-12 in 6-well cell culture dishes (Millicell® Cell Culture Inserts, Millipore, Darmstadt, Germany). At this step, the retinas were incubated with drops of virus solution (lentivirus or rAAV) to allow for the transduction with the shRNA virus. Retinas of postnatal day 0 mice were cultured for at least 10-12 days at 37°C in 5% CO_2. After fixation in paraformaldehyde, specimens were embedded, cryosectioned and further processed for immunohistochemistry and electron microscopy.

Acknowledgements

We thank Beata Schmidt and Nadja Gießl for excellent technical assistance.

Competing interests

The authors declare no competing or financial interests.

Author contributions

Conceptualization: A.G.; Methodology: N.F., K.K., S.-F.S., K.B., E.B., H.R.-L., M.U., C.T.T., R.R., A.G.; Validation: A.G.; Formal analysis: N.F., K.K., K.B., R.R., A.G.; Investigation: N.F., K.K., A.G.; Resources: E.B., S.M., A.A.N., C.T.T., A.G.; Writing - original draft: N.F., A.G.; Writing - review & editing: K.K., E.B., R.R., J.H.B., A.G.; Supervision: A.G.; Project administration: A.G.; Funding acquisition: A.G.

Funding

We acknowledge support from the Deutsche Forschungsgemeinschaft (GI 770 1-1/1-2) and the Charlotte & Tistou Kerstan Foundation.

Supplementary information

Supplementary information available online at
http://jcs.biologists.org/lookup/doi/10.1242/jcs.218487.supplemental

References

Adams, M., Smith, U. M., Logan, C. V. and Johnson, C. A. (2008). Recent advances in the molecular pathology, cell biology and genetics of ciliopathies. *J. Med. Genet.* **45**, 257-267.

Avasthi, P. and Marshall, W. F. (2012). Stages of ciliogenesis and regulation of ciliary length. *Differentiation* **83**, S30-S42.

Becirovic, E., Böhm, S., Nguyen, O. N. P., Riedmayr, L. M., Hammelmann, V., Schön, C., Butz, E. S., Wahl-Schott, C., Biel, M. and Michalakis, S. (2016). AAV vectors for FRET-based analysis of protein-protein interactions in photoreceptor outer segments. *Front. Neurosci.* **10**, 356.

Boldt, K., van Reeuwijk, J., Lu, Q., Koutroumpas, K., Nguyen, T.-M. T., Texier, Y., van Beersum, S. E. C., Horn, N., Willer, J. R., Mans, D. A. et al. (2016). An organelle-specific protein landscape identifies novel diseases and molecular mechanisms. *Nat. Commun.* **7**, 11491.

Buchman, J. J., Tseng, H.-C., Zhou, Y., Frank, C. L., Xie, Z. and Tsai, L.-H. (2010). Cdk5rap2 interacts with pericentrin to maintain the neural progenitor pool in the developing neocortex. *Neuron* **66**, 386-402.

Chen, D., Purohit, A., Halilovic, E., Doxsey, S. J. and Newton, A. C. (2004). Centrosomal anchoring of protein kinase C betaII by pericentrin controls microtubule organization, spindle function, and cytokinesis. *J. Biol. Chem.* **279**, 4829-4839.

Chen, C.-T., Hehnly, H., Yu, Q., Farkas, D., Zheng, G., Redick, S. D., Hung, H.-F., Samtani, R., Jurczyk, A., Akbarian, S. et al. (2014). A unique set of centrosome proteins requires pericentrin for spindle-pole localization and spindle orientation. *Curr. Biol.* **24**, 2327-2334.

Cooper, B., Hemmerlein, M., Ammermuller, J., Imig, C., Reim, K., Lipstein, N., Kalla, S., Kawabe, H., Brose, N., Brandstatter, J. H. et al. (2012). Munc13-independent vesicle priming at mouse photoreceptor ribbon synapses. *J. Neurosci.* **32**, 8040-8052.

Croci, C., Brandstätter, J. H. and Enz, R. (2003). ZIP3, a new splice variant of the PKC-zeta-interacting protein family, binds to GABAC receptors, PKC-zeta, and Kv beta 2. *J. Biol. Chem.* **278**, 6128-6135.

Dafinger, C., Liebau, M. C., Elsayed, S. M., Hellenbroich, Y., Boltshauser, E., Korenke, G. C., Fabretti, F., Janecke, A. R., Ebermann, I., Nürnberg, G. et al. (2011). Mutations in KIF7 link Joubert syndrome with Sonic Hedgehog signaling and microtubule dynamics. *J. Clin. Invest.* **121**, 2662-2667.

Dawe, H. R., Smith, U. M., Cullinane, A. R., Gerrelli, D., Cox, P., Badano, J. L., Blair-Reid, S., Sriram, N., Katsanis, N., Attie-Bitach, T. et al. (2007). The Meckel-Gruber Syndrome proteins MKS1 and meckelin interact and are required for primary cilium formation. *Hum. Mol. Genet.* **16**, 173-186.

Dawe, H. R., Adams, M., Wheway, G., Szymanska, K., Logan, C. V., Noegel, A. A., Gull, K. and Johnson, C. A. (2009). Nesprin-2 interacts with meckelin and mediates ciliogenesis via remodelling of the actin cytoskeleton. *J. Cell Sci.* **122**, 2716-2726.

del Bene, F., Wehman, A. M., Link, B. A. and Baier, H. (2008). Regulation of neurogenesis by interkinetic nuclear migration through an apical-basal notch gradient. *Cell* **134**, 1055-1065.

Delaval, B. and Doxsey, S. J. (2010). Pericentrin in cellular function and disease. *J. Cell Biol.* **188**, 181-190.

Doxsey, S. J., Stein, P., Evans, L., Calarco, P. D. and Kirschner, M. (1994). Pericentrin, a highly conserved centrosome protein involved in microtubule organization. *Cell* **76**, 639-650.

Endoh-Yamagami, S., Karkar, K. M., May, S. R., Cobos, I., Thwin, M. T., Long, J. E., Ashique, A. M., Zarbalis, K., Rubenstein, J. L. R. and Peterson, A. S. (2010). A mutation in the pericentrin gene causes abnormal interneuron migration to the olfactory bulb in mice. *Dev. Biol.* **340**, 41-53.

Espigat-Georger, A., Dyachuk, V., Chemin, C., Emorine, L. and Merdes, A. (2016). Nuclear alignment in myotubes requires centrosome proteins recruited by nesprin-1. *J. Cell Sci.* **129**, 4227-4237.

Falk, N., Lösl, M., Schröder, N. and Gießl, A. (2015). Specialized cilia in mammalian sensory systems. *Cells* **4**, 500-519.

Flory, M. R. and Davis, T. N. (2003). The centrosomal proteins pericentrin and kendrin are encoded by alternatively spliced products of one gene. *Genomics* **82**, 401-405.

Gilliam, J. C., Chang, J. T., Sandoval, I. M., Zhang, Y., Li, T., Pittler, S. J., Chiu, W. and Wensel, T. G. (2012). Three-dimensional architecture of the rod sensory cilium and its disruption in retinal neurodegeneration. *Cell* **151**, 1029-1041.

Gillingham, A. K. and Munro, S. (2000). The PACT domain, a conserved centrosomal targeting motif in the coiled-coil proteins AKAP450 and pericentrin. *EMBO Rep.* **1**, 524-529.

Gloeckner, C. J., Boldt, K., Schumacher, A., Roepman, R. and Ueffing, M. (2007). A novel tandem affinity purification strategy for the efficient isolation and characterisation of native protein complexes. *Proteomics* **7**, 4228-4234.

Gonçalves, J., Nolasco, S., Nascimento, R., Fanarraga, M. L., Zabala, J. C. and Soares, H. (2010). TBCCD1, a new centrosomal protein, is required for centrosome and Golgi apparatus positioning. *EMBO Rep.* **11**, 194-200.

Gotthardt, K., Lokaj, M., Koerner, C., Falk, N., GIEßl, A. and Wittinghofer, A. (2015). A G-protein activation cascade from Arl13B to Arl3 and implications for ciliary targeting of lipidated proteins. *eLife* **4**, e11859.

Graser, S., Stierhof, Y.-D., Lavoie, S. B., Gassner, O. S., Lamla, S., Le Clech, M. and Nigg, E. A. (2007). Cep164, a novel centriole appendage protein required for primary cilium formation. *J. Cell Biol.* **179**, 321-330.

Greer, Y. E., Westlake, C. J., Gao, B., Bharti, K., Shiba, Y., Xavier, C. P., Pazour, G. J., Yang, Y. and Rubin, J. S. (2014). Casein kinase 1delta functions at the centrosome and Golgi to promote ciliogenesis. *Mol. Biol. Cell* **25**, 1629-1640.

Griffith, E., Walker, S., Martin, C.-A., Vagnarelli, P., Stiff, T., Vernay, B., Al Sanna, N., Saggar, A., Hamel, B., Earnshaw, W. C. et al. (2008). Mutations in pericentrin cause Seckel syndrome with defective ATR-dependent DNA damage signaling. *Nat. Genet.* **40**, 232-236.

Gustafsdottir, S. M., Schallmeiner, E., Fredriksson, S., Gullberg, M., Söderberg, O., Jarvius, M., Jarvius, J., Howell, M. and Landegren, U. (2005). Proximity ligation assays for sensitive and specific protein analyses. *Anal. Biochem.* **345**, 2-9.

Jurczyk, A., Gromley, A., Redick, S., Agustin, J. S., Witman, G., Pazour, G. J., Peters, D. J. M. and Doxsey, S. (2004). Pericentrin forms a complex with intraflagellar transport proteins and polycystin-2 and is required for primary cilia assembly. *J. Cell Biol.* **166**, 637-643.

Kamiya, A., Tan, P. L., Kubo, K., Engelhard, C., Ishizuka, K., Kubo, A., Tsukita, S., Pulver, A. E., Nakajima, K., Cascella, N. G. et al. (2008). Recruitment of PCM1 to the centrosome by the cooperative action of DISC1 and BBS4: a candidate for psychiatric illnesses. *Arch. Gen. Psychiatry* **65**, 996-1006.

Koch, S., Sothilingam, V., Garcia Garrido, M., Tanimoto, N., Becirovic, E., Koch, F., Seide, C., Beck, S. C., Seeliger, M. W., Biel, M. et al. (2012). Gene therapy restores vision and delays degeneration in the CNGB1-/- mouse model of retinitis pigmentosa. *Hum. Mol. Genet.* **21**, 4486-4496.

Kracklauer, M. P., Banks, S. M. L., Xie, X., Wu, Y. and Fischer, J. A. (2007). Drosophila klaroid encodes a SUN domain protein required for Klarsicht localization to the nuclear envelope and nuclear migration in the eye. *Fly (Austin)* **1**, 75-85.

Leal-Ortiz, S., Waites, C. L., Terry-Lorenzo, R., Zamorano, P., Gundelfinger, E. D. and Garner, C. C. (2008). Piccolo modulation of Synapsin1a dynamics regulates synaptic vesicle exocytosis. *J. Cell Biol.* **181**, 831-846.

Li, Q., Hansen, D., Killilea, A., Joshi, H. C., Palazzo, R. E. and Balczon, R. (2001). Kendrin/pericentrin-B, a centrosome protein with homology to pericentrin that complexes with PCM-1. *J. Cell Sci.* **114**, 797-809.

Lu, W., Schneider, M., Neumann, S., Jaeger, V.-M., Taranum, S., Munck, M., Cartwright, S., Richardson, C., Carthew, J., Noh, K. et al. (2012). Nesprin interchain associations control nuclear size. *Cell. Mol. Life Sci.* **69**, 3493-3509.

Lüke, Y., Zaim, H., Karakesisoglou, I., Jaeger, V. M., Sellin, L., Lu, W., Schneider, M., Neumann, S., Beijer, A., Munck, M. et al. (2008). Nesprin-2 Giant (NUANCE) maintains nuclear envelope architecture and composition in skin. *J. Cell Sci.* **121**, 1887-1898.

Malone, C. J., Misner, L., Le Bot, N., Tsai, M. C., Campbell, J. M., Ahringer, J. and White, J. G. (2003). The C. elegans hook protein, ZYG-12, mediates the essential attachment between the centrosome and nucleus. *Cell* **115**, 825-836.

Mikule, K., Delaval, B., Kaldis, P., Jurcyzk, A., Hergert, P. and Doxsey, S. (2007). Loss of centrosome integrity induces p38-p53-p21-dependent G1-S arrest. *Nat. Cell Biol.* **9**, 160-170.

Miyoshi, K., Asanuma, M., Miyazaki, I., Matsuzaki, S., Tohyama, M. and Ogawa, N. (2006a). Characterization of pericentrin isoforms in vivo. *Biochem. Biophys. Res. Commun.* **351**, 745-749.

Miyoshi, K., Onishi, K., Asanuma, M. P., Miyazaki, I., Diaz-Corrales, F. J. and Ogawa, N. (2006b). Embryonic expression of pericentrin suggests universal roles in ciliogenesis. *Dev. Genes Evol.* **216**, 537-542.

Miyoshi, K., Kasahara, K., Miyazaki, I., Shimizu, S., Taniguchi, M., Matsuzaki, S., Tohyama, M. and Asanuma, M. (2009). Pericentrin, a centrosomal protein related to microcephalic primordial dwarfism, is required for olfactory cilia assembly in mice. *FASEB J.* **23**, 3289-3297.

Morris, N. R. (2003). Nuclear positioning: the means is at the ends. *Curr. Opin. Cell Biol.* **15**, 54-59.

Mühlhans, J. and Gießl, A. (2012). Pericentrin in health and disease: exploring the patchwork of Pericentrin splice variants. *Commun. Integr. Biol.* **5**, 304-307.

Mühlhans, J., Brandstätter, J. H. and GIEßl, A. (2011). The centrosomal protein pericentrin identified at the basal body complex of the connecting cilium in mouse photoreceptors. *PLoS ONE* **6**, e26496.

Patterson, K., Molofsky, A. B., Robinson, C., Acosta, S., Cater, C. and Fischer, J. A. (2004). The functions of Klarsicht and nuclear lamin in developmentally regulated nuclear migrations of photoreceptor cells in the Drosophila eye. *Mol. Biol. Cell* **15**, 600-610.

Piane, M., Della Monica, M., Piatelli, G., Lulli, P., Lonardo, F., Chessa, L. and Scarano, G. (2009). Majewski osteodysplastic primordial dwarfism type II (MOPD II) syndrome previously diagnosed as Seckel syndrome: report of a novel mutation of the PCNT gene. *Am. J. Med. Genet. A* **149A**, 2452-2456.

Rajgor, D. and Shanahan, C. M. (2013). Nesprins: from the nuclear envelope and beyond. *Expert Rev. Mol. Med.* **15**, e5.

Rauch, A., Thiel, C. T., Schindler, D., Wick, U., Crow, Y. J., Ekici, A. B., van Essen, A. J., Goecke, T. O., Al-Gazali, L., Chrzanowska, K. H. et al. (2008). Mutations in the pericentrin (PCNT) gene cause primordial dwarfism. *Science* **319**, 816-819.

Regus-Leidig, H., Fuchs, M., Löhner, M., Leist, S. R., Leal-Ortiz, S., Chiodo, V. A., Hauswirth, W. W., Garner, C. C. and Brandstätter, J. H. (2014). In vivo knockdown of Piccolino disrupts presynaptic ribbon morphology in mouse photoreceptor synapses. *Front. Cell Neurosci.* **8**, 259.

Roepman, R. and Wolfrum, U. (2007). Protein networks and complexes in photoreceptor cilia. *Subcell. Biochem.* **43**, 209-235.

Söderberg, O., Gullberg, M., Jarvius, M., Ridderstråle, K., Leuchowius, K.-J., Jarvius, J., Wester, K., Hydbring, P., Bahram, F., Larsson, L.-G. et al. (2006). Direct observation of individual endogenous protein complexes in situ by proximity ligation. *Nat. Methods* **3**, 995-1000.

Srsen, V., Gnadt, N., Dammermann, A. and Merdes, A. (2006). Inhibition of centrosome protein assembly leads to p53-dependent exit from the cell cycle. *J. Cell Biol.* **174**, 625-630.

Tibelius, A., Marhold, J., Zentgraf, H., Heilig, C. E., Neitzel, H., Ducommun, B., Rauch, A., Ho, A. D., Bartek, J. and Krämer, A. (2009). Microcephalin and pericentrin regulate mitotic entry via centrosome-associated Chk1. *J. Cell Biol.* **185**, 1149-1157.

Tsai, L.-H. and Gleeson, J. G. (2005). Nucleokinesis in neuronal migration. *Neuron* **46**, 383-388.

Tsujikawa, M., Omori, Y., Biyanwila, J. and Malicki, J. (2007). Mechanism of positioning the cell nucleus in vertebrate photoreceptors. *Proc. Natl. Acad. Sci. USA* **104**, 14819-14824.

Wheway, G., Schmidts, M., Mans, D. A., Szymanska, K., Nguyen, T. T., Racher, H., Phelps, I. G., Toedt, G., Kennedy, J., Wunderlich, K. A. et al. (2015). An siRNA-based functional genomics screen for the identification of regulators of ciliogenesis and ciliopathy genes. *Nat. Cell Biol.* **17**, 1074-1087.

Willems, M., Genevieve, D., Borck, G., Baumann, C., Baujat, G., Bieth, E., Edery, P., Farra, C., Gerard, M., Heron, D. et al. (2010). Molecular analysis of pericentrin gene (PCNT) in a series of 24 Seckel/microcephalic osteodysplastic primordial dwarfism type II (MOPD II) families. *J. Med. Genet.* **47**, 797-802.

Yu, J., Lei, K., Zhou, M., Craft, C. M., Xu, G., Xu, T., Zhuang, Y., Xu, R. and Han, M. (2011). KASH protein Syne-2/Nesprin-2 and SUN proteins SUN1/2 mediate nuclear migration during mammalian retinal development. *Hum. Mol. Genet.* **20**, 1061-1073.

Zahnleiter, D., Hauer, N. N., Kessler, K., Uebe, S., Sugano, Y., Neuhauss, S. C. F., Gießl, A., Ekici, A. B., Blessing, H., Sticht, H. et al. (2015). MAP4-dependent regulation of microtubule formation affects centrosome, cilia, and golgi architecture as a central mechanism in growth regulation. *Hum. Mutat.* **36**, 87-97.

Zebrowski, D. C., Vergarajauregui, S., Wu, C. C., Piatkowski, T., Becker, R., Leone, M., Hirth, S., Ricciardi, F., Falk, N., GIEßl, A. et al. (2015). Developmental alterations in centrosome integrity contribute to the post-mitotic state of mammalian cardiomyocytes. *eLife* **4**, e05563.

Zhang, Q., Ragnauth, C. D., Skepper, J. N., Worth, N. F., Warren, D. T., Roberts, R. G., Weissberg, P. L., Ellis, J. A. and Shanahan, C. M. (2005). Nesprin-2 is a multi-isomeric protein that binds lamin and emerin at the nuclear envelope and forms a subcellular network in skeletal muscle. *J. Cell Sci.* **118**, 673-687.

Zhang, X., Lei, K., Yuan, X., Wu, X., Zhuang, Y., Xu, T., Xu, R. and Han, M. (2009). SUN1/2 and Syne/Nesprin-1/2 complexes connect centrosome to the nucleus during neurogenesis and neuronal migration in mice. *Neuron* **64**, 173-187.

Zimmerman, W. C., Sillibourne, J., Rosa, J. and Doxsey, S. J. (2004). Mitosis-specific anchoring of gamma tubulin complexes by pericentrin controls spindle organization and mitotic entry. *Mol. Biol. Cell* **15**, 3642-3657.